Journal of Sedimentary Research

Journal of Sedimentary Research, 2006, v. 76, 1012–1034
Research Article
DOI: 10.2110/jsr.2006.083

MARINE ISOTOPE STAGE 6 CANYON AND SPILLOVER DEPOSITS OF THE BRYANT AND EASTERN CANYON SYSTEMS, NORTHWEST GULF OF MEXICO: IMPORTANCE OF FINE-GRAINED TURBIDITES ON A DELTA-FED PROGRADING SLOPE

EFTHYMIOS K. TRIPSANAS,[1,2] WILLIAM R. BRYANT,[1] NIALL C. SLOWEY,[1] AND JIN WOOK KIM[3]
[1]*Department of Oceanography, Texas A&M University, Texas 77843, U.S.A.*
[2]*Bedford Institute of Oceanography, Dartmouth, Nova Scotia B2Y 4A2, Canada*
[3]*Naval Research Laboratory, NASA Stennis Space Center, Mississippi 39529, U.S.A.*
e-mail: etripsan@nrcan.gc.ca

ABSTRACT: **A large set of long sediment cores and high-resolution seismic-reflection data were used to study the sedimentology of the delta-fed prograding slope of the northwest Gulf of Mexico, during Marine Isotope Stage (MIS) 6 (125–180 ka). Bryant and Eastern canyon systems were the main pathways during this period through which Mississippi River sediment was delivered down the continental slope.**

Two MIS 6 sedimentary environments have been defined on the slope of the northwest Gulf of Mexico: intracanyon and overbank environments. The erosional action of turbidity currents in Bryant and Eastern canyons was focused mainly on the thalweg, whereas, on the rest of the canyon floors, the flows acquired a mainly depositional character, resulting in the formation of inner levees and terraces. MIS 6 deposits in overbank environments consist entirely of thick ($>$ 50 m), widespread ($>$ 15–20 km), and continuous successions of mud turbidites, which indicate that spillover processes were dominant along Bryant and Eastern canyons. The total absence of bioturbation structures and hemipelagic sediments in MIS 6 overbank deposits indicate high sedimentation rates exceeding 200–600 cm/ky.

The majority of the overbank deposits are normally graded, indicating that most of the turbidity currents during MIS 6 resulted from sediment failures on the outer shelf and upper continental slope. Sedimentological observations indicate that a complete mud turbidite sequence (T0–8 sequence in the nomenclature of Stow and Shanmugam 1980) results from a waning low-density turbidity current consisting of four successive flow-regime stages: (1) an initial erosional stage ($\geq$ 30 cm/s), (2) deposition of the coarsest, noncohesive fraction (silt) of the suspended sediment in the flows (30–100 cm/s), (3) cyclic deposition of cohesive (mud) and noncohesive (silt) laminae due to fluctuations in the shear stress in the boundary layer of the flow (12–30 cm/s), and (4) deposition from a silt-depleted and slowly moving ($\leq$ 15 cm/s) sediment cloud.

INTRODUCTION

Spillover of turbidity currents is an important process that has been studied mainly on submarine fans (Peakall et al. 2000). On submarine fans, turbidity currents are usually thicker than the depth of the channels. This leads to the confinement of only the coarser and denser lower part of the turbidity currents within the channels, whereas their upper and more dilute part overflows the channel levees and spills onto the interchannel or overbank areas. Spillover processes are responsible for the construction of channel levees (Skene et al. 2002) and large mud waves on the overbank areas (Normark et al. 2002). Levee deposits usually consist of thin-bedded sand and/or silt and mud turbidites that with distance from the channel become thinner and finer grained (silt and clay; Piper 1978; Stow et al. 1984; Normark et al. 1993; Bouma 2000). Spillover of turbidity currents is intensified on bends of channels, where inertial and centrifugal forces lead to superelevation and the separation of the upper part of the turbidity currents (Bowen et al. 1984; Piper and Savoye 1993; Peakall et al. 2000). This process contributes to the formation of crevasse splays, channel bifurcation, and avulsion (Piper and Normark 1983; Savoye et al. 1993).

Spillover processes on continental slopes have received very little attention, due to the general assumption that turbidity currents are totally confined within submarine canyons, with hemipelagic sedimentation to dominate on the intercanyon areas. However, small levees, overbank deposits, and mud waves have been reported adjacent to some canyons (e.g., meandering submarine canyon systems along the Peru–Chile forearc, Hagen et al. 1994; Ebro Canyons, Nelson and Maldonado 1990). This implies that spillover flows may have played a more active role in the sedimentation of continental slopes than was initially thought.

This paper reports the results of a detailed sedimentological study of sediment cores (up to 20 m long) and high-resolution seismic-reflection data from the Bryant and Eastern canyon systems, located on the prograding continental slope of the northwest Gulf of Mexico (Fig. 1). Both canyon systems are characterized by extensive Marine Isotope Stage (MIS) 6 (125–180 ka) overbank deposits, consisting entirely of silt–mud turbidites, and therefore, offer a rare opportunity for the study of fine-grained overbank deposits from canyons. The main purpose of this study is to provide a better insight in the flow characteristics and depositional processes of canyon-contained and spillover MIS 6 turbidity currents, to determine the connective link between the deposits of these two flow types, and in extension, to identify slope progradation processes on overbank canyon areas.

 1527-1404/06/076-1012/$03.00

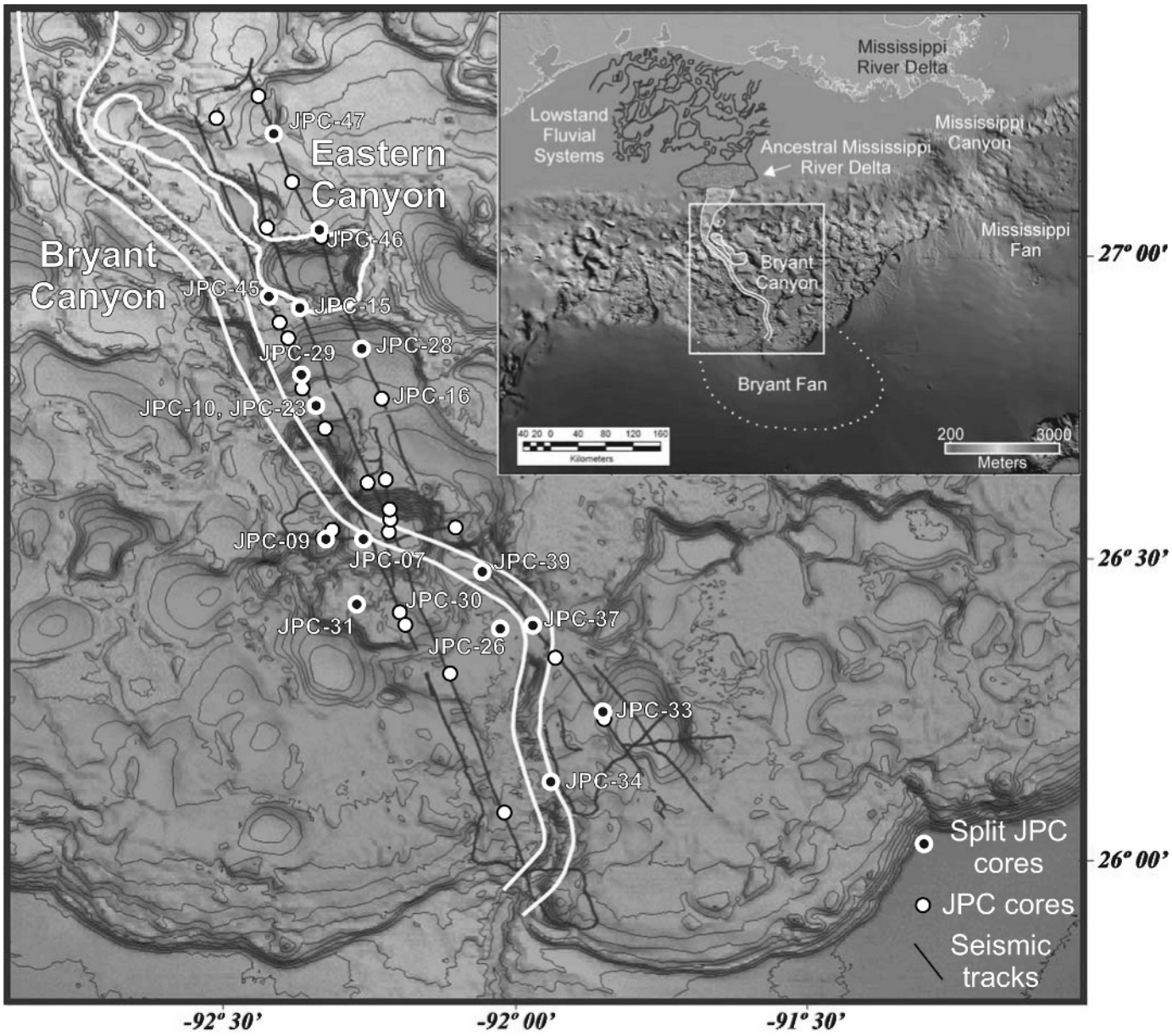

FIG. 1.— Shaded bathymetric maps of the Bryant Canyon area and the northwest Gulf of Mexico displaying the locations of the jumbo piston cores (JPC), the acquisition tracks of the high-resolution geophysical information, and the locations of Bryant and Eastern canyon systems at MIS 6 (adapted from Lee et al. 1996 and Twichell et al. 2000), along with an ancient lowstand fluvial system on the shelf and an ancestral Mississippi River Delta (adapted from Suter and Berryhill 1985). The white lines indicate the pathways of Bryant and Eastern canyons. Contours represent isobaths at 100 m intervals.

GEOLOGICAL SETTING

Halokinetic processes have resulted in the hummocky topography of the northwest continental slope of the Gulf of Mexico, which consists of uplifts caused by salt domes, ridges, and sheets with intervening salt-withdrawal basins (Fig. 1). The diapirs originate from the Middle and Upper Jurassic Luann Salt, which is overlain by thick Cretaceous and Cenozoic sediments. Bryant et al. (1990) identified the presence of over 90 intraslope salt-withdrawn mini-basins in the Northwest Gulf of Mexico with a relief in excess of 150 m. Many intraslope basins originated from the diapiric blockage of abandoned canyon systems (Bouma et al. 1990). The most significant abandoned canyon systems are Bryant and Eastern canyons, which have been deformed by halokinetic processes into a network of intraslope mini-basins separated by sills or plateaus (shallow salt structures; Lee 1990). Bryant Canyon can be traced from the shelf margin to the lower continental slope, where it passes basinwards into the well-developed Bryant Fan on the continental rise (Lee et al. 1996; Twichell et al. 2000). Eastern Canyon is confined to the upper continental slope and terminates in a prominent intraslope basin (Twichell et al. 2000). It is unclear whether Eastern Canyon was once a branch of Bryant Canyon, or if it was an isolated autonomous canyon system.

Lee et al. (1996) and Twichell et al. (2000) have described the formation and destruction of the Bryant and Eastern canyon systems. These systems were initiated at the beginning of MIS 6 (penultimate glacial episode; Tripsanas et al. in press), by the development of an ancestral shelf-margin Mississippi River Delta (Suter and Berryhill 1985) that led to the generation of numerous gravity flows on the slope. Initially, gravity flows propagated downslope and developed a small erosional canyon on the

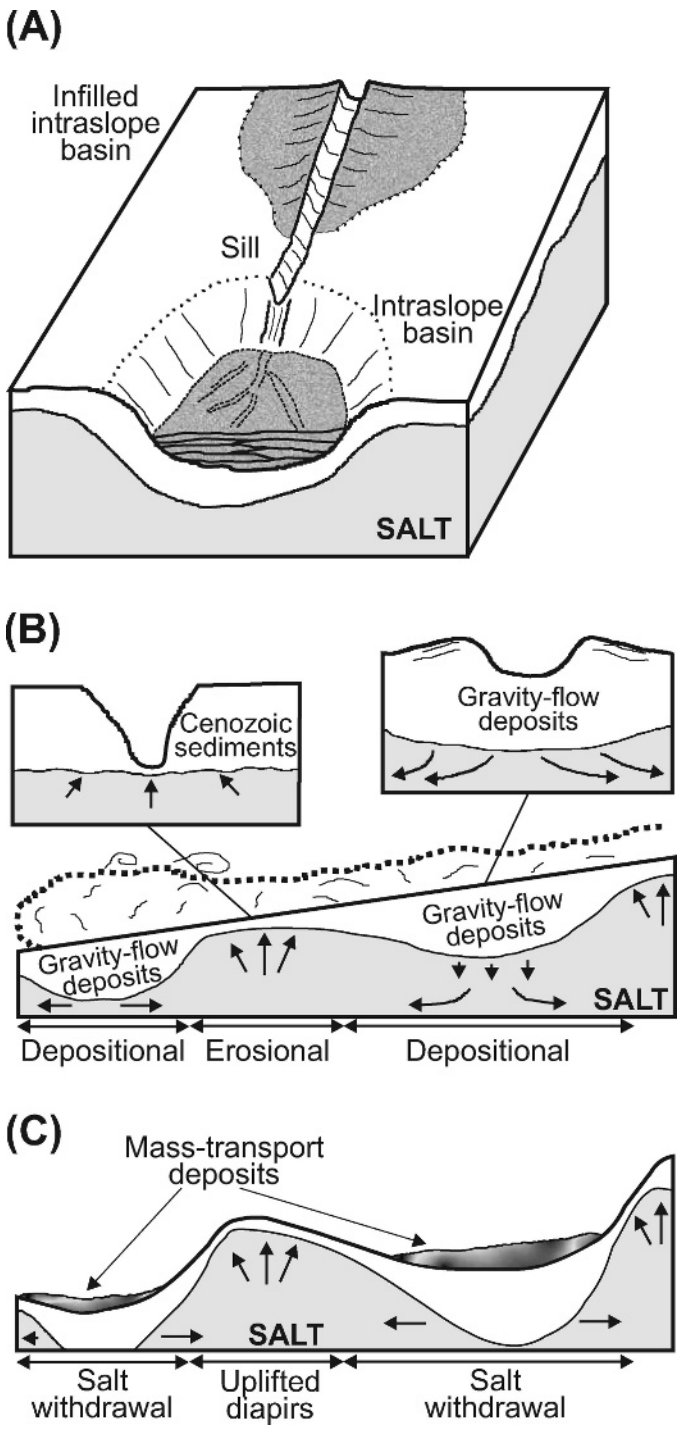

FIG. 2.—Cartoon of the formation and destruction of the Bryant and Eastern canyon systems (modified from Twichell et al. 2000). **A)** Sketch of the canyons displaying the infilling–bypassing process that resulted in their formation. **B)** Bryant Canyon during its full development, displaying the equilibrium between the salt mobilization and the erosional and depositional processes of the bypassing turbidity currents. **C)** Sketch of the canyons after their abandonment and transformation by halokinetic processes.

upper continental slope (Berryhill 1981). Because of the highly irregular morphology of the continental slope, the gravity flows were eventually confined in the most proximal intraslope basins, and formed ponded intraslope–intrabasinal fan systems (channel–levee complexes and sheet sands). When the intraslope basins were filled to a certain level, the gravity flows spilled and propagated to the most adjacent, downdip intraslope basins, resulting in a downdip shift of the ponded fan facies (Lee et al. 1996; Twichell et al. 2000) (Fig. 2A). Repetitions of this fill-and-spill process led to the peculiar structure of Bryant and Eastern canyon systems, which in the infilled intraslope basins had the form of well-developed channel–levee turbidite systems, and on the sills, separating the basins, had the form of typical V-shaped erosional canyons (Lee 1990; Satterfield and Behrens 1990; Twichell et al. 2000) (Fig. 2A, B).

Erosion and sedimentation within the canyons destabilized the underlying salt because of differential sediment loading. Uplifting salt diapirs tended to obliterate and restore the seafloor morphology along the erosional parts of the canyons, whereas salt withdrawal and subsidence occurred along their depositional parts (Lee 1990; Lee et al. 1996; Twichell et al. 2000). However, coupled erosion of sills and deposition in basins balanced the salt movements during MIS 6 (Fig. 2B) (Lee et al. 1996; Twichell et al. 2000). The re-subsidence of the infilled basins, resulting in the high relief (~ 500 m) of Bryant and Eastern canyons, occurred after their abandonment at the beginning of the interglacial MIS 5 (Fig. 2C) (Tripsanas 2003). The cessation of turbidity currents was due to the confinement of river-derived sediment on the wide continental shelf of the northwest Gulf of Mexico after sea level rose (Suter et al. 1987). The deformation of the canyon systems resulted in the production of numerous sediment failures through the oversteepening of the slopes (Twichell et al. 2000; Tripsanas et al. 2004). Mass-transport deposits represent the latest infilling of the canyons along the intraslope basins.

STRATIGRAPHY

Tripsanas (2003) distinguished four upper Quaternary sedimentary units in the Bryant Canyon area, through the sedimentological analysis of long (< 20 m) piston cores, coupled with ^{14}C AMS dates and oxygen-isotope curves. These sediments were deposited during Marine Isotope Stages (MIS) 1–6. Starting with the youngest sedimentary unit, they are (Figs. 3, 4):

- Unit 1 (0.20–3.35 m thick) consists of heavily bioturbated, muddy foraminifera ooze, and represents hemipelagic sediments of Holocene age (MIS 1).
- Unit 2 (3.20–14.80 m thick) consists of bioturbated muddy foraminifera ooze that is interbedded with clayey-mud turbidites. This unit represents deposits of the last glaciation (MIS 2–4). The absence of sand and silt turbidites in this unit is attributed to the deformation along the canyons pathway, resulting in sills with up to 500 m relief that separated the intraslope basins (Twichell et al. 2000). The intraslope basins resulted in the entrapment of the coarse material of the turbidity currents in the upper continental slope, with only their upper, finer-grained and dilute clouds able to propagate downslope to the core sites. In addition, during the last glaciation, the main Mississippi River discharges had shifted to the east, cutting off most of previous MIS 6 sediment supply. Sediment supply in the Bryant Canyon area during the last glaciation was significant only during periods of exceptionally high Mississippi River discharge (Tripsanas et al. in press).
- Unit 3 (1.20–5.50 m thick) consists of heavily bioturbated muddy foraminifera ooze, which contains the Y-8 ash layer, dated at 84 ka (Rabek et al. 1985). This unit represents hemipelagic deposits of the interglacial MIS 5.
- Unit 4 (more than 10.00 m thick) consists of sand and mud turbidites within the canyons and entirely of mud turbidites on the overbank areas of the canyons. This unit represents deposits of the penultimate glaciation (MIS 6). The upper contact of unit 4 ranges from gradational to sharp. The sharp contact indicates the occurrence of

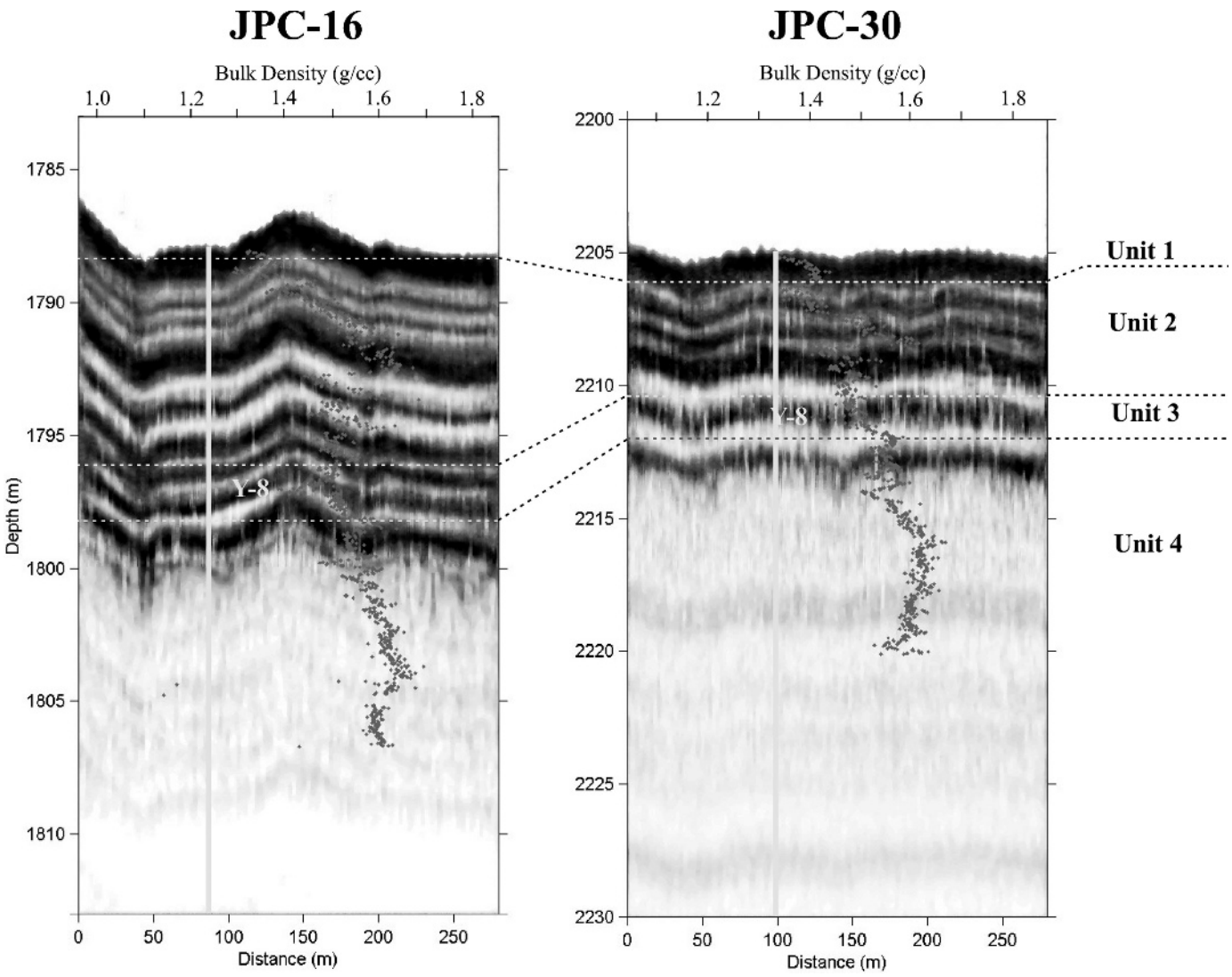

FIG. 3.—3.5 kHz sub-bottom profiles and bulk-density profiles from two typical JPC cores from the Bryant Canyon area (locations are shown in Fig. 4).

thin sediment failures, which resulted from the deformation of Bryant and Eastern canyons pathways at the beginning of the interglacial MIS 5.

In 3.5 kHz profiles (Fig. 3), units 1–3 display sharp, continuous, and conformable or parallel reflectors, whereas the acoustic character of unit 4 ranges from a semi-transparent zone to prolonged echoes with no further penetration (see section of seismic characterization of MIS 6 deposits below). Unit 4 (core recovery ranging from 0.2 to 10 m thick) is present in 24 out of the 48 total piston cores of this study. The penetration was not deep enough to recover MIS 6 sediments in 10 cores, and 14 other cores recovered only MIS 1–5 mass-transport deposits (Tripsanas et al. 2004; Tripsanas et al. in press).

DATA AND METHODS

High-resolution acoustic data were collected from the Bryant Canyon area during the R/V Gyre 1998 cruise, using the Texas A&M Deep-Tow system, which is equipped with a 3.5 kHz echo sounder, and a 100 kHz side-scan sonar towed thirty meters above the seafloor (Fig. 1). Forty-eight Jumbo piston cores (JPC) up to 20 m long were acquired from thirty-eight different locations in floors and overbank areas of Bryant and Eastern canyons, using the Woods Hole Oceanographic Institution (WHOI) Jumbo Piston Corer during a cruise in 1998 of the R/V Knorr (Fig. 1, Appendix A).

Bulk-density and P-wave velocity profiles were measured from all cores with a GEOTEK Multi-Sensor Core Logger. Eighteen split sediment cores were described at millimeter scale and photographed on high-resolution film. High-resolution X-ray radiographs were also taken from 1-cm-thick sediment slabs along the entire length of the cores. The core descriptions, photographs, and X-radiographs were used to select sedimentary units for grain-size analysis. The sand fraction was removed from the samples by wet sieving, and the sand grain-size distribution was determined by dry sieving. The analyses of the silt and clay fractions were performed by the use of a Sedigraph and Coulter Counter and reported using the Wentworth scale (clay < 4 μm). Impregnated samples, thin sections, and numerous smear slides were also produced in order to study the structures and mineralogy of the sediments using SEM analysis and standard optical petrographic techniques. The sedimentological analysis and interpretation of the remaining 30 cores was based solely on their bulk-density and P-wave velocity profiles. The ages of the sediments were determined by radiocarbon dating on planktonic foraminifera tests

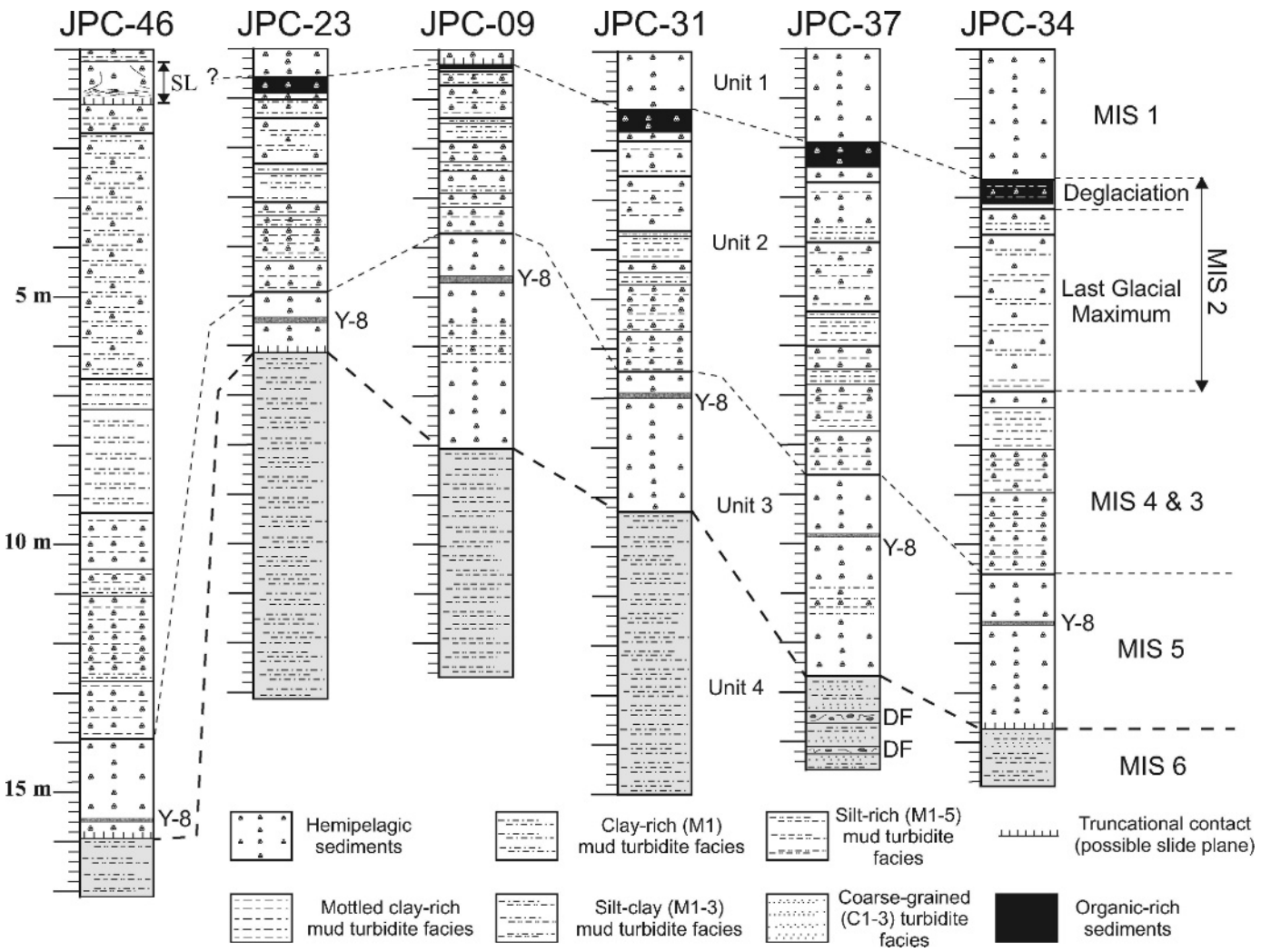

FIG. 4.—Sedimentological descriptions of six cores from the upper to lower continental slope. Locations are shown in Figure 1. SL=slump, DF=debris flow.

(*Globigerinoides ruber*) and from oxygen-isotope curves derived from planktonic foraminifera (*Globigerinoides ruber*) in two representative cores (JPC-31 and JPC-46) (Tripsanas et al. in press).

CLASSIFICATION OF 3.5 KHZ SEISMIC FACIES

Classification and mapping of 3.5 kHz seismic facies were used to help reconstruct the sedimentary environments of the Bryant Canyon area during MIS 6. Six 3.5 kHz seismic facies are recognized (Table 1).

Seismic facies I represents MIS 5-1 hemipelagic deposits with a few interbeds of mud turbidites (sedimentary units 1–3). Facies I is ubiquitous throughout the continental slope and is absent only at locations that have been influenced by slope instability processes (slumps, slides, debris flows, etc.). Seismic facies II, III, and IV are directly related to the canyon environments (Fig. 5) and are interpreted to be MIS 6 deposits (sedimentary unit 4). Facies II occurs exclusively along the pathway of Bryant Canyon, and represents sandy and silty deposits in the canyon floor. Facies III occurs all around the Eastern Canyon, whereas along the Bryant Canyon it occurs only on the outer banks of two canyon bends. Facies III represents overbank deposits of layered mud interbedded with a few thin silt laminae. Facies IV comprises the remainder of the Bryant Canyon area and consists exclusively of layered mud. The thickness of seismic facies II, III, and IV exceeds the sound penetration of the 3.5 kHz sub-bottom profiles (< 50 m). The seismic character of facies III and IV does not remain constant, but their reflections gradually decrease in amplitude away from the canyon pathways (Fig. 6). This echo character suggests that the sedimentary units become finer grained away from the canyons (Damuth 1980).

Seismic facies V is interpreted to represent areas influenced by slope instability processes. Sediment failures occur preferentially in intraslope basins, along the pathways of the canyons. Their origin is probably from the halokinetic deformation of the canyons pathway beginning in MIS 5 (Tripsanas et al. in press). Seismic facies VI occurs in areas that have been influenced by gas hydrates and significant faulting adjacent to the canyon and mini-basin walls, where extensive uplift of salt diapirs has occurred.

CLASSIFICATION OF SEDIMENTARY FACIES

MIS 6 deposits from the Bryant Canyon area consist of successive turbidite facies, characterized by the complete absence of interbedded hemipelagic sediments. Intercanyon (overbank) areas comprise entirely mud (fine-grained) turbidites, which consist of five facies depending on their sedimentary characteristics (Table 2; Figs. 7–10). Intracanyon deposits are composed of successions of fine- and coarse-grained turbidites, which comprise three sedimentary facies (Table 3).

TABLE 1.—*Classification of 3.5 kHz seismic facies recognized in profiles from the Bryant Canyon area.*

3.5 kHz Seismic Facies	Interpretation[1]	Examples
Seismic facies I Sharp to semi-prolonged, parallel, continuous reflections.	Marine Isotope Stage 5 to 1 hemipelagic sediments. MIS 4, 3, and 2 deposits are interbedded with a few mud turbidites and/or contourites	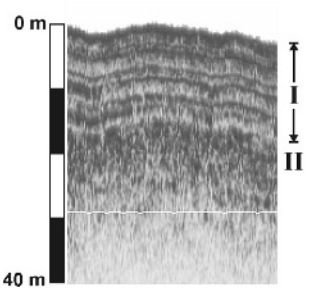
Seismic facies II Very prolonged echoes with no internal reflections or rare semi-prolonged discontinuous reflections.	Mud layers interbedded with closely spaced sand and silt layers deposited during Marine Isotope Stage 6	
Seismic facies III Distinct, sharp, parallel, continuous reflections of high to low amplitude.	Mud layers interbedded with a few thin (< 2 mm) silt laminae deposited during Marine Isotope Stage 6	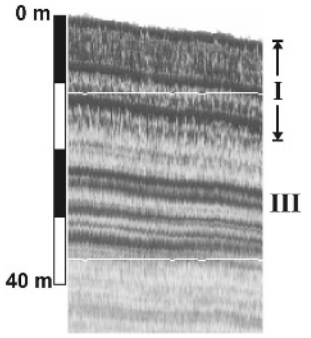
Seismic facies IV Distinct, sharp, parallel, continuous reflections of low amplitude.	Layered mud deposited during Marine Isotope Stage 6	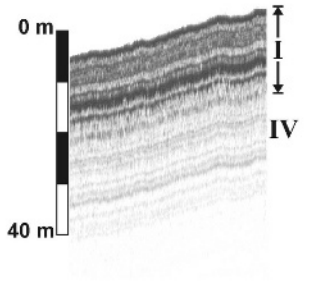
Seismic facies V Sharp to prolonged irregular bottom echoes. Transparent to chaotic internal seismic facies with lenticular or wedging external shape. This facies occurs in depressions of a hummocky acoustic basement, or within stratified sediments.	Slump and debris-flow deposits, evacuation zones	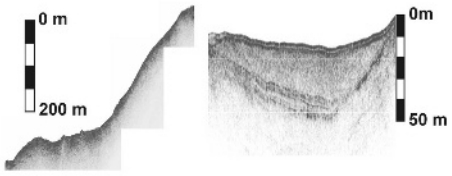
Seismic facies VI Indistinct to prolonged reflections with wipe-out zones and highly inclined planes of low-reflectivity offsetting reflectors.	Gas hydrates, faulted areas, liquefaction zones (preferentially along fault planes)	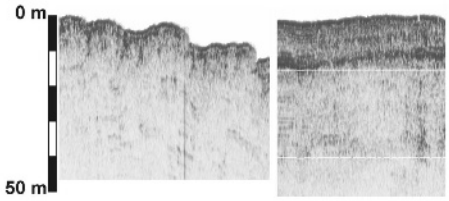

[1]The interpretation of the seismic facies was based on sediment core analysis (see later in text), and the 3.5 kHz seismic classification of Damuth (1980).

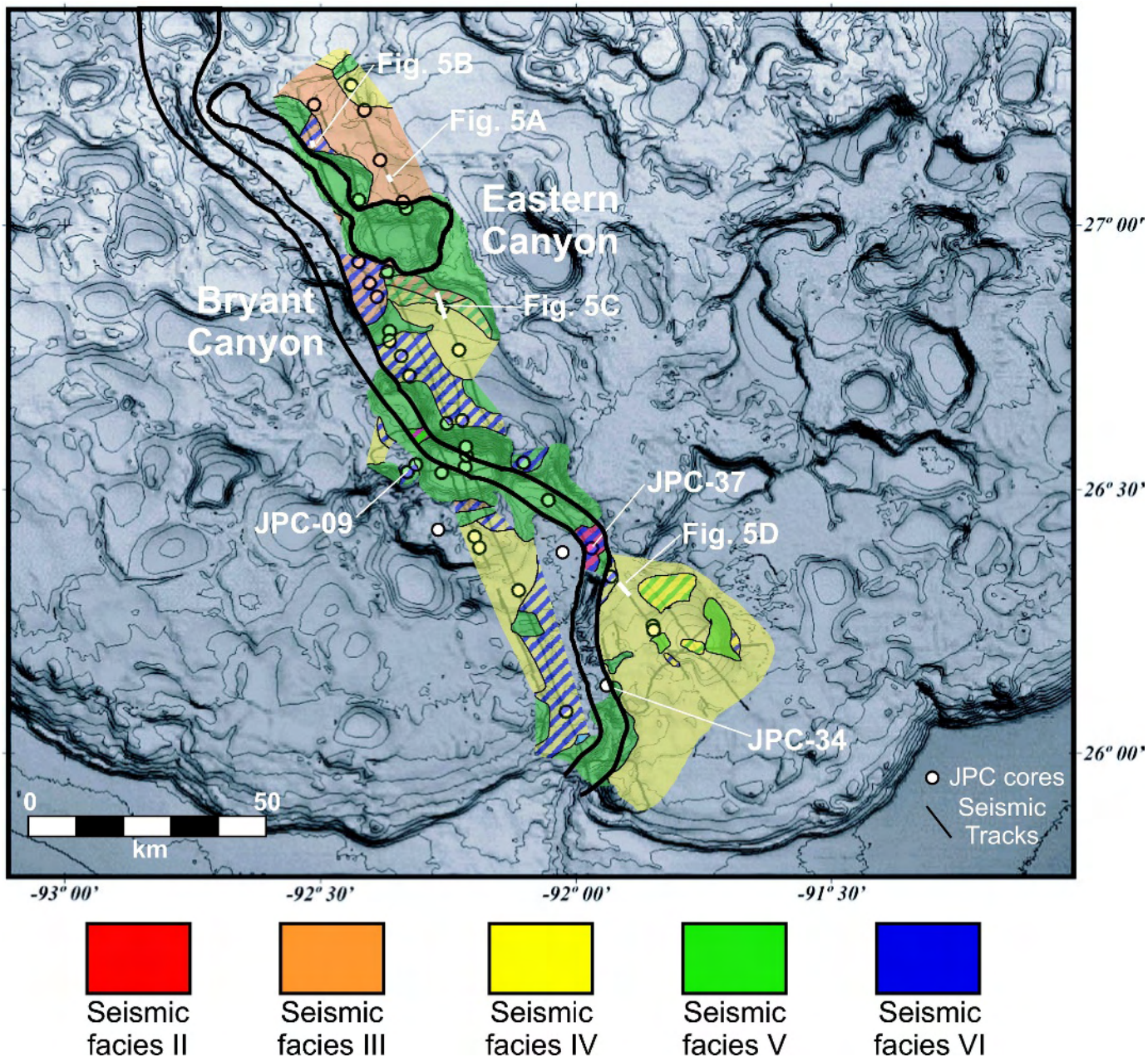

FIG. 5.—Distribution of 3.5 kHz seismic facies in the Bryant Canyon area that represent deposits of the penultimate glaciation (MIS 6). Striped patterns represent mixed or closely alternating seismic facies. The heavy black lines outline the pathways of Bryant and Eastern canyons.

Mud turbidite facies consist of two grain-size populations (Figs. 8, 10): a coarser grain population composed of the fraction of coarse to fine silt, and a finer grain population that comprises the fraction of very fine silt and clay. The coarser grain population dominates in facies M5 and M4, is significantly reduced in facies M3 and M2, and is totally replaced by the finer grain population in facies M1. The coarser grain population reveals a general fining and depleting trend, moving from the coarser (M5 and M4) towards the finer mud facies (M1–3). Inversely, the finer grain population gradually becomes dominant in the finer mud facies, exhibiting an almost constant mode, ranging between 7.5 and 8.5 phi (5.5–2.7 μm). The only exception is observed in two facies of a characteristic red color (facies M4a in Fig. 10), where the mode ranged between 9 and 9.5 phi (2–1.4 μm), suggesting a different sediment source. Similar observations on the behavior of the two grain-size populations are also apparent upward within the facies (normal grading in Fig. 10).

Mud turbidite facies similar to the mud turbidite facies observed in the Bryant and Eastern canyons have been reported worldwide. The most detailed study is from the Halifax Formation, Canada, by Stow et al. (1984), who described similar mud turbidite facies. Reexamination of data from the Mississippi Fan (DSDP leg 96: Bouma et al. 1986) reveals that almost the entire spectrum of mud facies described in this study also occurs on overbank and distal areas of the Mississippi Fan. Mud turbidite facies M1, M2, and M3 have also been reported from the coarse-grained Monterey Fan on an overbank mud-wave field (Normark et al. 1980). Facies M1 and M2 have been repeatedly documented from the Eastern

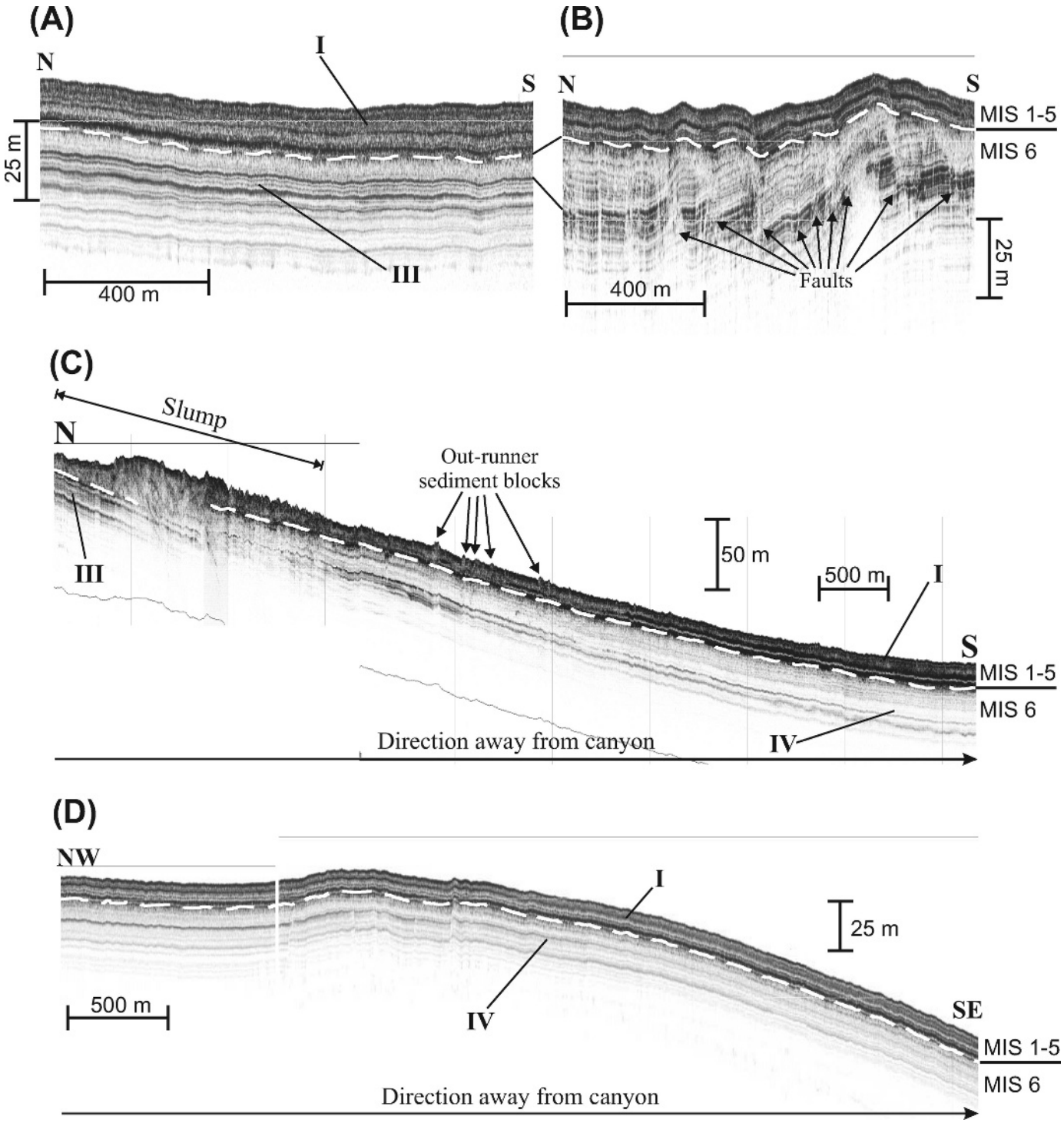

FIG. 6.—3.5 kHz sub-bottom profiles from the overbank areas of Bryant and Eastern canyons. Locations are shown in Figure 5.

Mediterranean (Stanley 1983), and they are interpreted to result from the depositional segregation (deposition of the coarser material in the most proximal topographic depressions) of large turbidity currents. On outer continental shelves and distal prodeltas like the Baie des Anges continental shelf influenced by Var and Paillon rivers (Klaucke et al. 2000), mud facies M1, M2, and M3 are very common, and they are interpreted to occur from hyperpycnal river plumes. The common occurrence of mud turbidite facies on a large spectrum of sedimentary environments reveals the importance for the better understanding of their sedimentology and depositional processes.

SPATIAL AND VERTICAL DISTRIBUTION OF THE TURBIDITE FACIES

The spatial distribution of the turbidite facies indicates two major sedimentological environments during the low sea-level stand of MIS 6 (Fig. 11): (1) the intracanyon areas of Bryant and Eastern canyon

TABLE 2.—*Sedimentological descriptions of mud turbidite facies, accompanied with typical examples of radiographs (negatives).*

Mud Turbidite Facies	Sedimentological Description
Facies M1 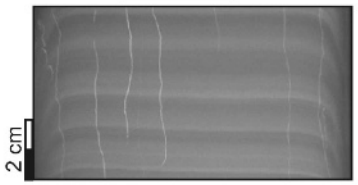	(beds a few mm up to 5 cm thick) Sharp-based, normally graded zone of clay that grades upward into a uniform lamina or layer of clay (silt/clay: 30/70 to 10/90). Upward within the normally graded zone, grain-size samples (S1-3 in Fig. 8) reveal higher percentages of particles with a diameter smaller than ~ 7-7.5 phi (7.8-5.5 μm). In many cases, these beds are characterized by a thin coarser silty-clay basal lamina (~ 1-3 mm) and/or the presence of fading-upwards, planar to wispy, faint, slightly siltier laminae. In some beds, a thin less silty interval underlies these silty laminae (Fig. 9A).
Facies M2 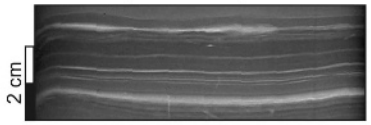	(beds 0.5 to several cm thick) Normally graded, sharp-based silty-clay beds (silt/clay: 20/80-40/60) characterized by a thin (1-3 mm) silt or clayey-silt basal lamina, and thin (< 1 mm) fading-upward, indistinct to wispy silty laminae. In some cases, they resemble facies M1 beds, except for the coarser-grained basal silt lamina. In a few beds, a thin less silty interval may underlie the basal silt (Fig. 9B).
Facies M3 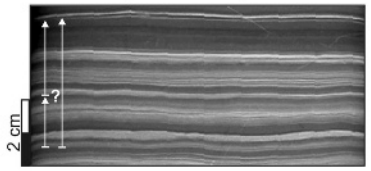	(beds 1 to several cm thick) Sharp-based, silty-clay beds (silt/clay: 40/60-55/45), characterized by thin (1-3 mm), parallel to wavy silt or clayey-silt laminae, which become indistinct to wispy upward and gradually fade away. The basal silt lamina is the thickest, and usually lenticular. In some cases, a few indistinct silty laminae may underlie the prominent basal silt.
Facies M4a 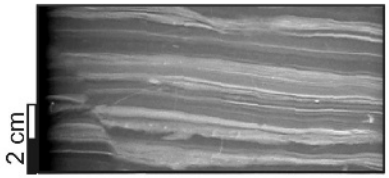 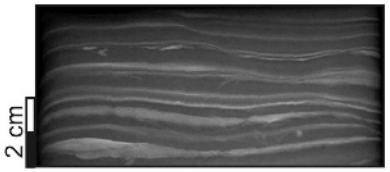	(beds 1 to several cm thick) Sharp-based beds, characterized by a basal zone of silty-clay with thick to thin (2-6 mm, and occasionally up to 1 cm) planar to lenticular silt laminae, which may be micro-laminated or even display small ripples of low amplitude and long wavelength, top fading ripples, and cross micro-laminations (silt/clay: 50/50-70/30). Most silty-clay laminae between the lenticular silt laminae are structureless. However, in some cases they include a few thin, small silt lenses and/or silty micro-laminae. Upward, the silt laminae become thinner, discontinuous and gradually fade away, or may pass sharply into a thin veneer of uniform silty clay. In a few beds, a few thinner and less silty laminae may precede these facies, developing an interval of inverse grading at their base (Fig. 9C).

TABLE 2.—*Continued.*

Facies 4b 	(beds 1 to several cm thick) Sharp-based and normally graded beds characterized by a thick basal zone (1-3 cm thick) of thin (1-3 mm), closely spaced, planar silt laminae (silt/clay: 60/40-70/30). Isolated, small climbing ripples may be developed at their base. Upward, the laminated basal zone is succeeded by either a uniform silty-clay thin layer, or a zone of fading-upward silt laminae. This facies is rare.
Facies 4c 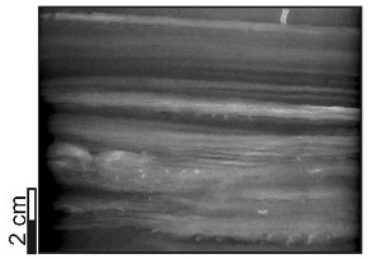	(beds 1 to several cm thick) Sharp- to gradationally based beds characterized by a silty (clayey silt to very silty silty clay) basal zone (1-3.5 cm thick), with thick silt lenses (0.3-1.5 cm thick) and small isolated ripples of low amplitude and long wavelength (silt/clay: 60/40-75/25). Upward, the silty basal zone either passes sharply into a uniform silty-clay layer (silt/clay: 55/45-35/65), or grades into a zone of fading-upward silt laminae. Very fine sand may be present in the silt lenses, but is generally less than 5%. In a few beds, a few thinner and less silty laminae underlie the basal zone, developing a short interval of inverse grading at the base of the bed. This facies is rare.
Facies M5a 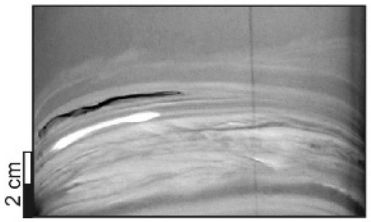	(beds 2 to several cm thick) Consists of a thin, basal lenticular silt layer (1-2.5 cm), which is planar to cross micro-laminated, and may display immature lensoid ripples, low-amplitude long-wavelength climbing ripples, and top fading ripples (silt/clay: 95/5-70/30). The base is sharp with common scouring (e.g. cut-and-fill structures). Basal silt layers are generally ungraded, but a few exhibit a normal or even inverse grading. The sand fraction is less than 5%. In some cases, a few silt laminae may underlie the sharp base of the bed. Upward, the silt basal layer is overlain by either a structureless silty-clay layer (0.5-2 cm thick; silt/clay: 55/45-35/65), or a zone of fading-upward silt laminae that in rare cases is caped by a uniform silty-clay layer.
Facies M5b 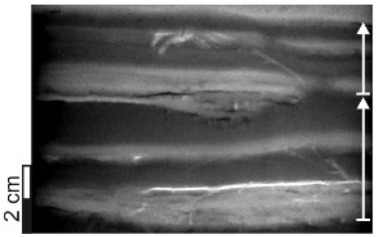	(beds 2 to several cm thick) Consists of a thick, normally graded, structureless, basal silt layer (0.5-1.5 cm; silt/clay: 90/10-70/30). At the top, the basal, structureless silt layer either passes sharply into a massive mud layer (0.5-2 cm thick; silt/clay: 55/45-35/65) or grades to a zone of fading-upwards silt laminae. The sand fraction is less than 5%. The bases of these beds are sharp with common scouring (e.g. cut-and-fill structures).

Loading structures such as necking, boudinage, distortion of the silt laminae, load casts, and small silt pseudonodules are common, and most apparent in facies M5 and M4 facies. Rare dewatering structures are also present in these facies.

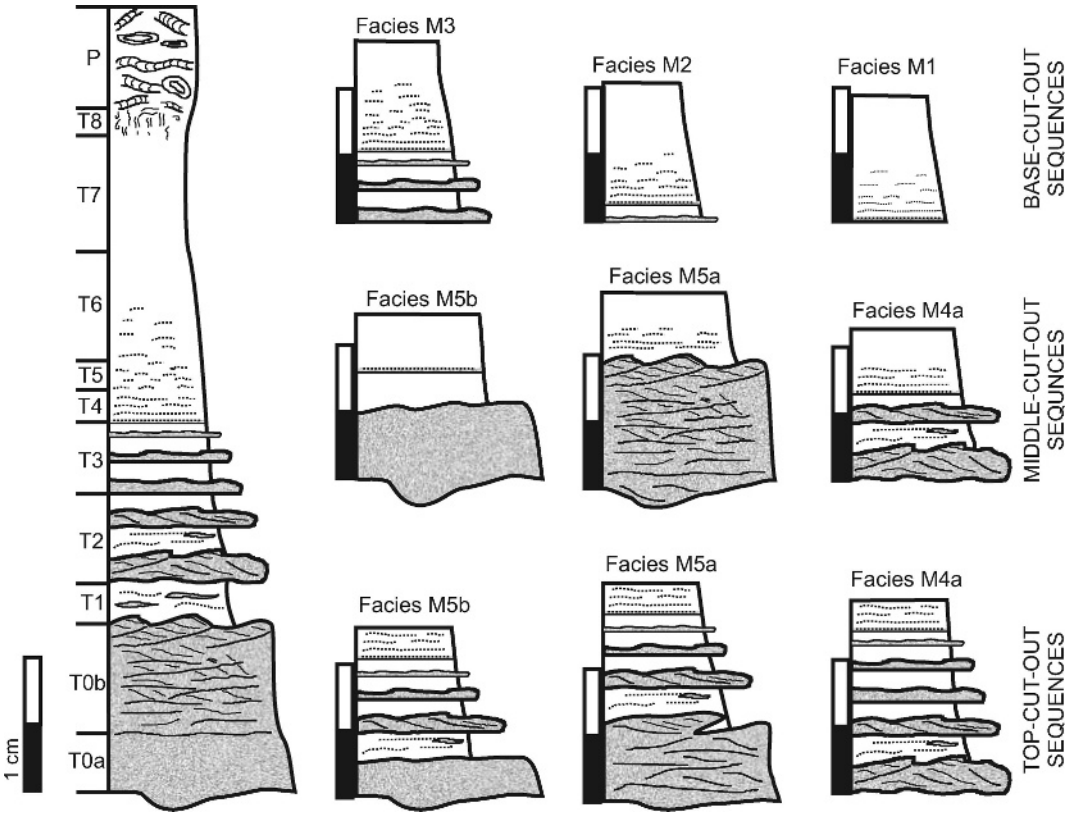

FIG. 7.—Graphic illustrations of the five mud turbidite facies distinguished in this study compared to the modified Stow and Shanmugam (1980) silt–mud turbidite sequence (shown at left). The mud turbidite facies are organized into three groups: top-cut-out sequences, middle-cut-out sequences, and base-cut-out sequences (modified from Stow et al. 1984).

systems, and (2) their surrounding areas subjected to spillover and flow-stripping processes (overbank areas).

Observations of sediments from intracanyon areas are based on cores JPC-37 (canyon floor) and JPC-34 (boundary of intracanyon and overbank areas). Both cores are located on the top of wide sills separating intraslope mini-basins, in which sediment failures are local and rare (Figs. 4, 5, 11; Tripsanas 2003). Sediments of the intracanyon environments consist of successions of M5 to M1 facies interbedded with coarse-grained turbidite facies C1 to C3. Intracanyon deposits are represented in 3.5 kHz sub-bottom profiles as seismic facies II (Table 1, Fig. 5).

The overbank areas of the canyon systems are divided into three areas (Fig. 11): (1) silt-rich overbank areas consisting of successions of mud turbidite facies M5 to M1 where facies M5 and M4 dominate, (2) silt–clay overbank areas comprising successions of facies M3 to M1, and (3) clay-rich overbank areas consisting of successions of facies M1 (rarely, facies M2 may occur in these deposits).

Deposits in silt-rich overbank areas have been recorded only in core JPC-09, located on the outer bank of bend B of Bryant Canyon (Figs. 5, 11). The seismic character of this area has been masked by the presence of gas hydrates. Silt–clay overbank areas are represented in 3.5 kHz profiles by seismic facies III (Table 1, Fig. 5), surround the entirety of Eastern Canyon, and along Bryant Canyon occur only on the outer banks of bends A and B. At bend B, silt–clay overbank deposits succeed silt-rich overbank deposits away from the canyon (Fig. 11). Clay-rich overbank areas surround the remainder of the Bryant Canyon system, whereas at bends and Eastern Canyon, such areas succeed the silt–clay overbank areas away from the canyons. In 3.5 kHz profiles, clay-rich overbank areas are represented by seismic facies IV (Table 1, Fig. 5).

The mud turbidite facies are organized into two types of series within all overbank areas (Fig. 12): (1) facies series revealing an upward-fining and thinning trend (fining series), and (2) fining series that are preceded by a short series of upward-coarsening and -thickening facies (coarsening–fining series). Hemipelagic sediments and bioturbation structures are absent to negligible in both intracanyon and overbank MIS 6 deposits.

DISCUSSION

Flow Processes of Mud Turbidite Facies

All mud turbidite facies represent top-cut-out (T0/2–3/4), middle-cut-out (T0/2, 6/7, or T2/3, 6/7), and base-cut-out (T3/4/5–7) silt–mud turbidite sequences according to the nomenclature of Stow and Shanmugam (1980) (Fig. 7). In a few rare cases, complete or nearly complete silt–mud turbidite sequences may also occur. We conclude from the sedimentological descriptions of this study and previous laboratory studies that mud-turbidite sequences (T0–7) are developed under four distinct flow-regime stages of a waning low-density turbidity current:

Stage 1.—The velocity and turbulent energy of the flows are sufficient to maintain all of its sediments in suspension, and to even incorporate seafloor sediments by erosion (Parker 1982; Fukushima et al. 1985; Kneller 1995). No deposition occurs in this flow regime, whereas scouring of the seafloor is common.

Stage 2.—A reduction in the velocity and turbulent energy of the flows leads to a decrease in the amount of sediment that can be maintained in suspension (loss of capacity), resulting in sediment deposition (Hiscott 1994). The settling sediment consists of silt particles and silt–clay flocs of equivalent settling velocities. However, floc breakage occurs in the boundary layer of the flows because of the strong shear, and the clay-size particles are reentrained into the main flows (McCave and Swift 1976;

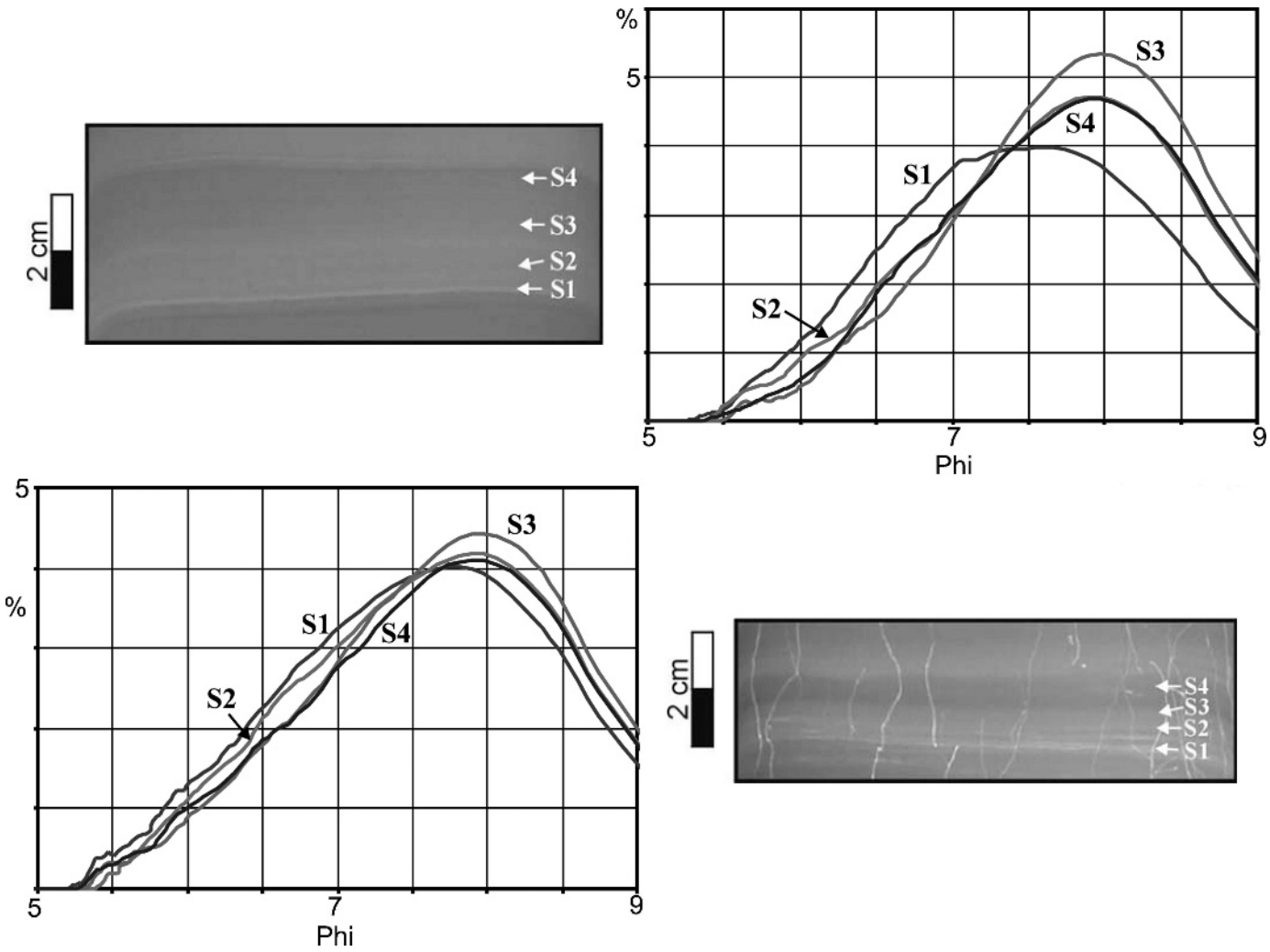

FIG. 8.—Weight % grain-size frequency curves from successive samples (~ 1 mm thick) of two discrete M1 mud turbidite beds. X-radiographs show sample locations.

Stow and Bowen 1980). This means the silt fraction is the main deposited material under these flow conditions. The silt basal zones of facies M5a and M5b (T0) are deposited in this stage. The structureless nature of the massive silt basal zones (T0a) of M5b facies indicate that they have been deposited under high sedimentation rates, during which hindered settling and dispersive pressures become dominant in the lower parts of the flows, thus leading to the suppression of any traction-induced structures (Allen 1991; Kneller and Branney 1995; Baas et al. 2000). Conversely, the planar to lenticular to ripple laminations in the silt basal zone (T0b) of the M5a facies imply that their deposition occurred under lower sedimentation rates and longer flow duration, allowing the development of tractional structures.

Stage 3.—Low-speed streaks, characterized by increased concentrations of sediment particles, have long been recognized as ubiquitous within the boundary layers of turbulent flows (McCave and Swift 1976; Hesse and Chough 1980; Allen 1985). One of the most important characteristics of the low-speed zones is the cyclic development of turbulent bursts, through which low-momentum fluid parcels are ejected back into the main flow. Sediments settling in the boundary layer are reentrained into the main flow through this cyclic streak-bursting mechanism. The frequency of the bursting events is directly related to the flow velocity and inversely related to the boundary-layer thickness (Allen 1985). Best and Leeder (1993) and Li and Gust (2000) have shown, through laboratory experiments, that cohesive sediment in the flows results in thickening of their boundary layers and decrease of the occurrence time period of the bursting events, and leads to significant reduction of the bottom drag of the flows. The directly measured shear velocities in the viscous sublayer could be reduced by as much as 70%.

As a low-density turbidity current decelerates (concomitant reduction of the bursting frequency), it eventually achieves a critical flow velocity, below which the amount of the aggregated cohesive sediments settling into the boundary layer exceeds the amount of the disaggregated cohesive sediments reentrained into the main flow. A refined version of the two-step depositional model of Stow and Bowen (1980) is proposed to occur under flow velocities below this critical value, and it is described in detail in Figure 13.

The lenticular, planar, indistinct, and wispy silt laminae of M4a, M3, and M2 facies (T2, 3, 4, 5) are developed during this flow-regime stage. The transition from the microlaminated lenticular silt laminae of division T2 to the indistinct and wispy silt laminae of divisions T4 and T5 among and within the mud facies is attributed to the gradual depletion of the silt population and deceleration of the low-density turbidity currents. The closely spaced silt laminae of facies M4b are interpreted to develop from silt-rich low-density turbidity currents that have relatively high velocities,

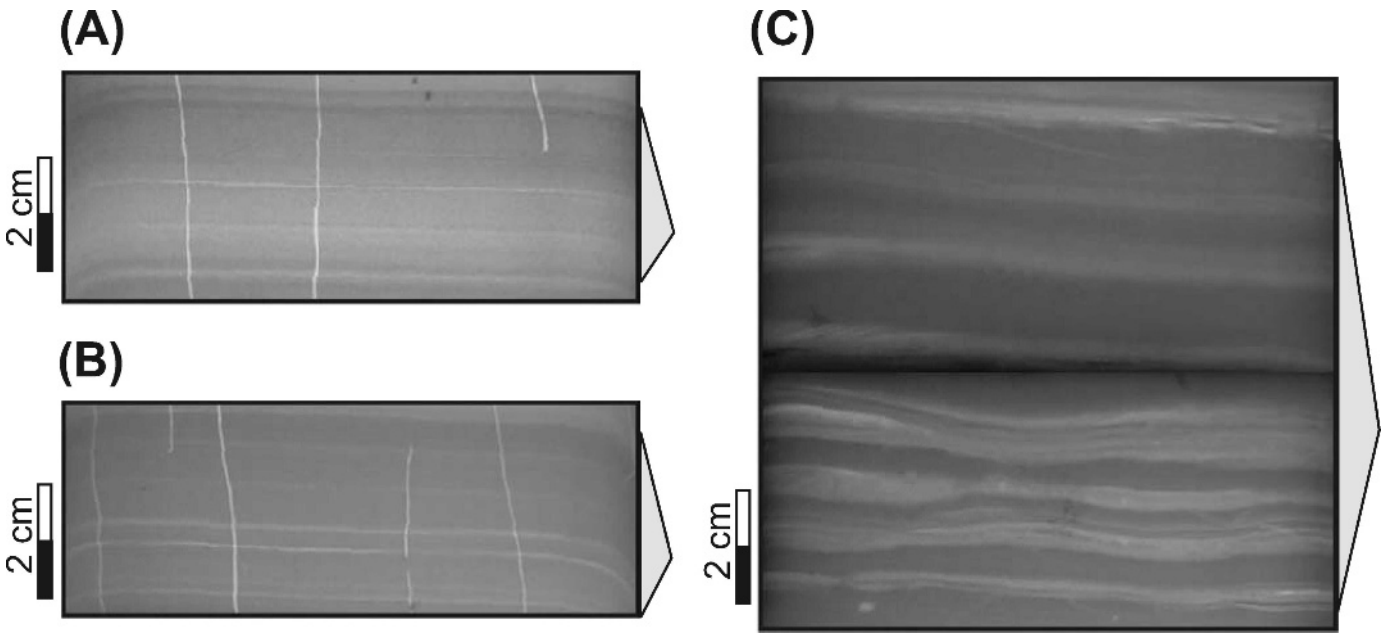

FIG. 9.—Inversely graded interval at base of beds in **A)** facies M1, **B)** M2/1, and **C)** M4 shown by X-radiographs (negatives). The triangle on the side indicates the location of the normally and inversely graded intervals of the beds. The dark band in the center of image (C) is an artifact.

which prohibit the formation of thick mud laminae. The lenticular silty basal zones of facies M4c are interpreted to have been deposited under transitional stage 2 to 3 flow regimes, yielding a poorly developed cyclic silt and mud deposition under high depositional rates.

Stage 4.—The graded M1 facies (T6, 7) are developed in this last stage. Deposition occurs from a clay-rich flow (≤ 30% of medium to fine silt), characterized by velocities below a threshold value, which allows the straight deposition of flocculated sediments. The normal grading in this facies is attributed to the gradual domination of settling aggregated sediments (finer than 7.8–5.5 μm with an almost constant mode of 5.5–2.7 μm) over the slowly accumulated silt grains on the seafloor. Sediment particles with diameter smaller than 7.8–5.5 μm are characterized by very small settling velocities, and can settle on the seafloor only as aggregates (Kranck 1975; Krone 1993; Winterwerp 2002). The effect of the cyclic reduction of the boundary-layer shear is greatly diminished in this stage, and is expressed only by the development of alternating siltier and more clayey laminae of clay. The normally graded zone (T6) of M1 facies grades upwards into a thin veneer of uniform clay (T7), which probably resulted from the deposition of a final very slowly moving (almost stationary) sediment cloud.

The normal grading of most of the mud turbidites in this study reveals that the majority of the low-density turbidity currents were of a waning nature, characterized by structural characteristics similar to those of typical surge-like turbidity currents: head, body, tail (Kneller and Buckee 2000; Mulder and Alexander 2001). Facies M5 and M4 are interpreted to have been deposited by low-density turbidity currents comprising all four flow stages. The absence of the upper divisions T4/5–7 in top-cut-out sequences of facies M5 and M4 are attributed to: (1) the bypassing of the finer-grained tails of the flows without depositing any material, and/or (2) the erosion of the tops of complete sequences by subsequent flows. Middle-cut-out sequences (T0/2, 7) are interpreted as typical deposits of surge-type turbidity currents, characterized by the absence of a body, passing sharply into the deposits of their slowly moving, almost stationary tails. Base-cut-out sequences (facies M3–M1) have resulted from the deposition of weaker flows (flow stages 3 to 4). The rare mud turbidite beds characterized by a short interval of inverse grading at their bases are interpreted to have been deposited from turbidity currents that were characterized by a short, waxing initial stage (waxing–waning flows in Mulder et al. 2003).

Flow Processes of Coarse-Grained Turbidite Facies

The laminated character of the facies C3 sand layer (upper-stage plane-bed formation) indicates that it was deposited under high flow velocities (Bridge 1978; Hesse and Chough 1980), where deposition due to flocculation was diminished by the high shear within the boundary layer. The closely spaced, silty-sand to sandy-silt laminae (T_d division) of C2 and C3 facies are interpreted to develop by cyclic depositional processes, similar to those that result in the deposition of the silt and mud laminae of the mud-turbidite facies. The close spacing of the laminae is attributed to the higher velocities of the turbidity currents and the higher settling rates of the sand and silt grain population.

The structureless and lenticular to rippled laminated silt zones of facies C1 resemble subdivisions T0a and T0b of the modified Stow and Shanmugam silt–mud turbidite sequence (Fig. 7), and therefore a similar depositional model is adopted for their formation. The basal poorly sorted structureless silt zone is deposited under exceptionally high sedimentation rates, constituting hindered settling and dispersive pressures dominant in the lower portions of the flows. Conversely, the better-sorted overlying laminated silt zone is deposited at a later stage under lower sedimentation rates that cause the re-domination of turbulence in the lower portion of the flows. Despite the similarities of the facies C1 silt deposits with T0a, 0b beds, their much larger thickness (up to 10 cm), total lack of grading, almost total lack of sand, and abundant dewatering structures indicate that facies C1 resulted from the rapid deposition of silt-rich flows that were probably of larger magnitude and concentration than those resulting in typical silt–mud turbidite sequences. The exclusive occurrence of facies C1 deposits in intracanyon environments substantiates the above conclusion.

Facies C1 and C3 grade from noncohesive sand and silt deposits emplaced at high flow velocities to cohesive deposits characteristic of low flow velocities. This strongly suggests that both facies have resulted from

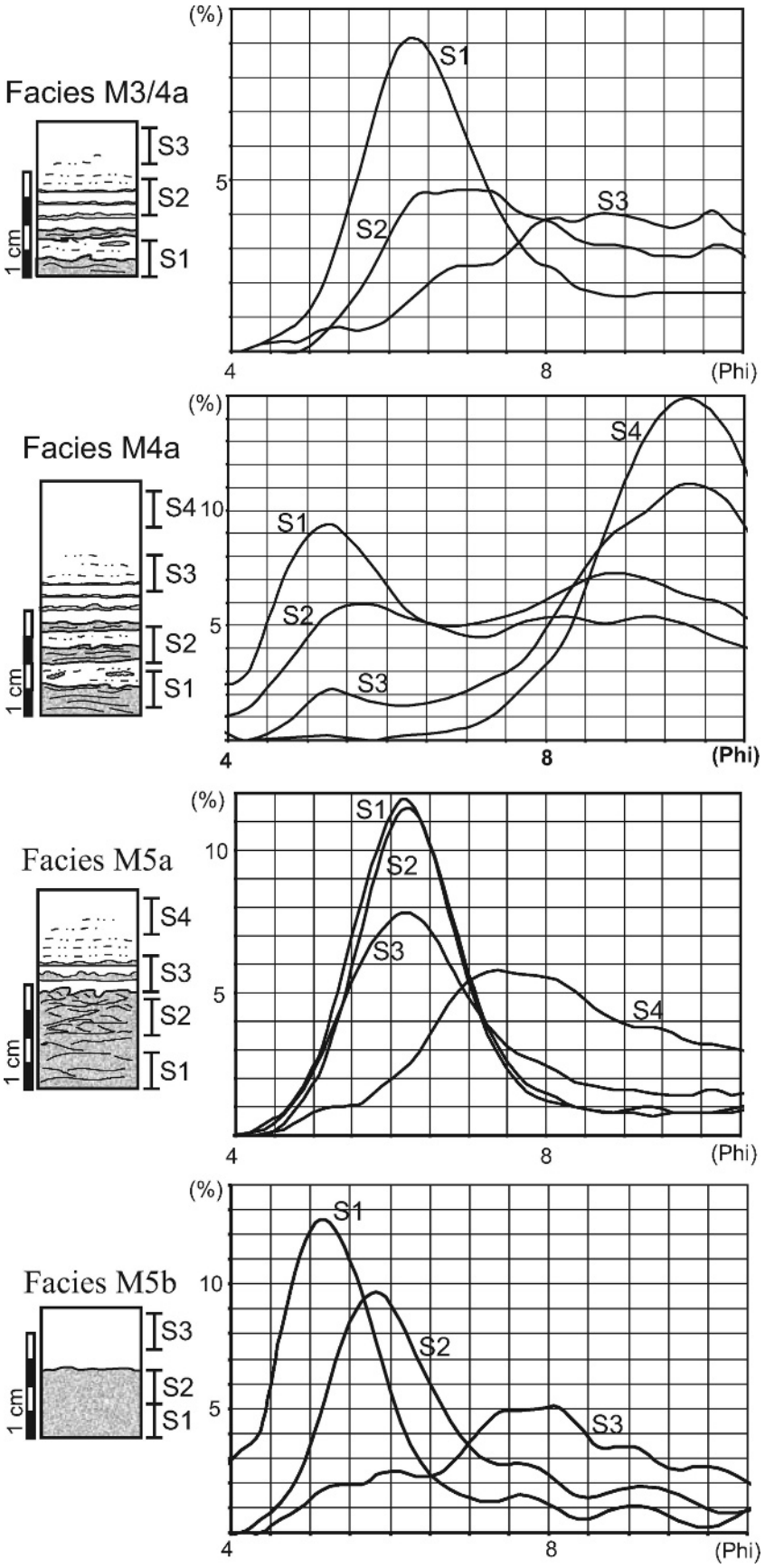

FIG. 10.— Weight % grain-size frequency curves from successive samples (~ 5 mm thick) of four discrete mud turbidite beds. Sediment logs show sample locations.

TABLE 3.—*Sedimentological descriptions, photographs (left), radiographs (right), and weight % grain-size frequency curves of coarse-grained turbidite facies.*

Coarse-Grained Turbidite Facies	Sedimentological Description
Facies C1 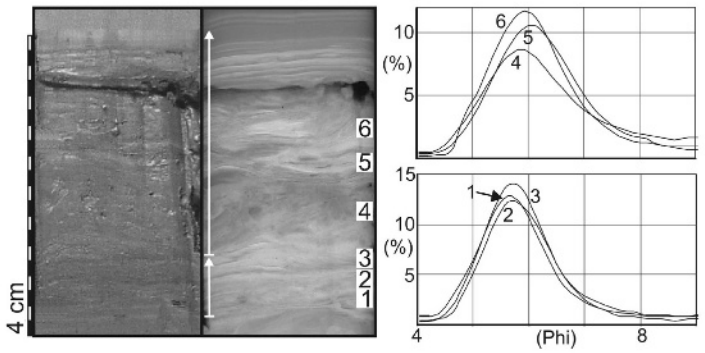	(beds a few to several cm thick) Consists of a structureless silt to clayey-silt basal zone (~ 70% silt) that is capped by a lenticular, wavy, rippled, and convolute-laminated, better-sorted silt layer (80-90 silt). The silt deposits reveal no distinct grading and are characterized by an almost constant mode in the grain-size frequency curves throughout the beds. The sand fraction is lower than 1%. The base of this unit is sharp with common scouring. Its top is either sharp to truncational overlain by a new silt turbidite facies, or it may gradually pass into finer-grained deposits of facies M4 or M3. Dewatering structures are very common and pervasive (especially in the basal structureless silt zone).
Facies C2 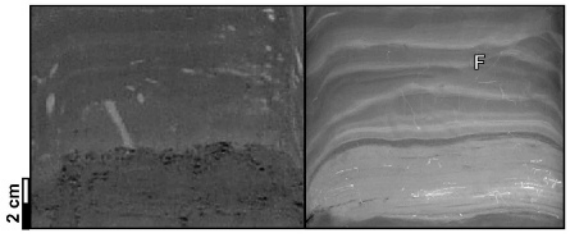	(beds a few to several cm thick; 20-50% sand, 40-65% silt, 10-15 % clay) Consists of closely spaced, silty sand to sandy silt and clayey silt to silty clay, planar to more rarely lenticular, alternating laminae. The base of the coarse basal zone is sharp and erosional. Its top may be sharp with indications of scouring (capped by another depositional event), or it may grade into finer-grained sediments resembling those of facies M4 or M3. This facies is equivalent to the $T_{d,e}$ partial Bouma sequence.
Facies C3 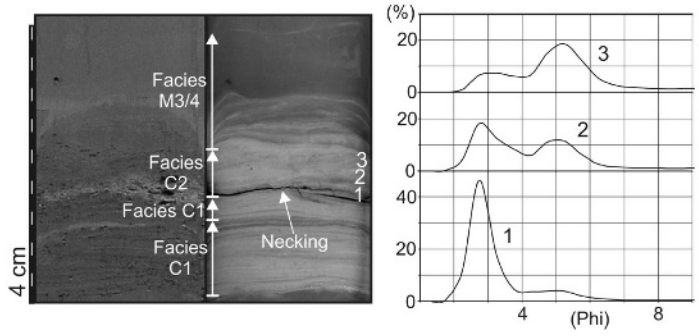	(beds a few to several cm thick). Similar to facies C2, with the only exception being that it is preceded at its base by a planar to lenticular to wavy laminated fine-sand layer (1 to a few cm thick; ~ 80% sand, ~ 15% silt, ~ 5% clay). This facies is equivalent to the $T_{b/c-e}$ partial Bouma sequence.
Loading structures such as necking, distortion, load casts, and pseudonodules are evident in all three facies.	

the deposition of fast-flowing, waning (surge-like) turbidity currents. The same conclusion is also assumed for the C2 facies. However, the silt and mud alternated laminae of the basal zone (T_d division) of facies C2 indicate that their deposition occurred from slower-moving and more diluted flows.

Intracanyon Environments

Sediments recovered in cores JPC-37 and JPC-34 from the Bryant Canyon floor consist of successions of C2 and M5 to M1 turbidite facies

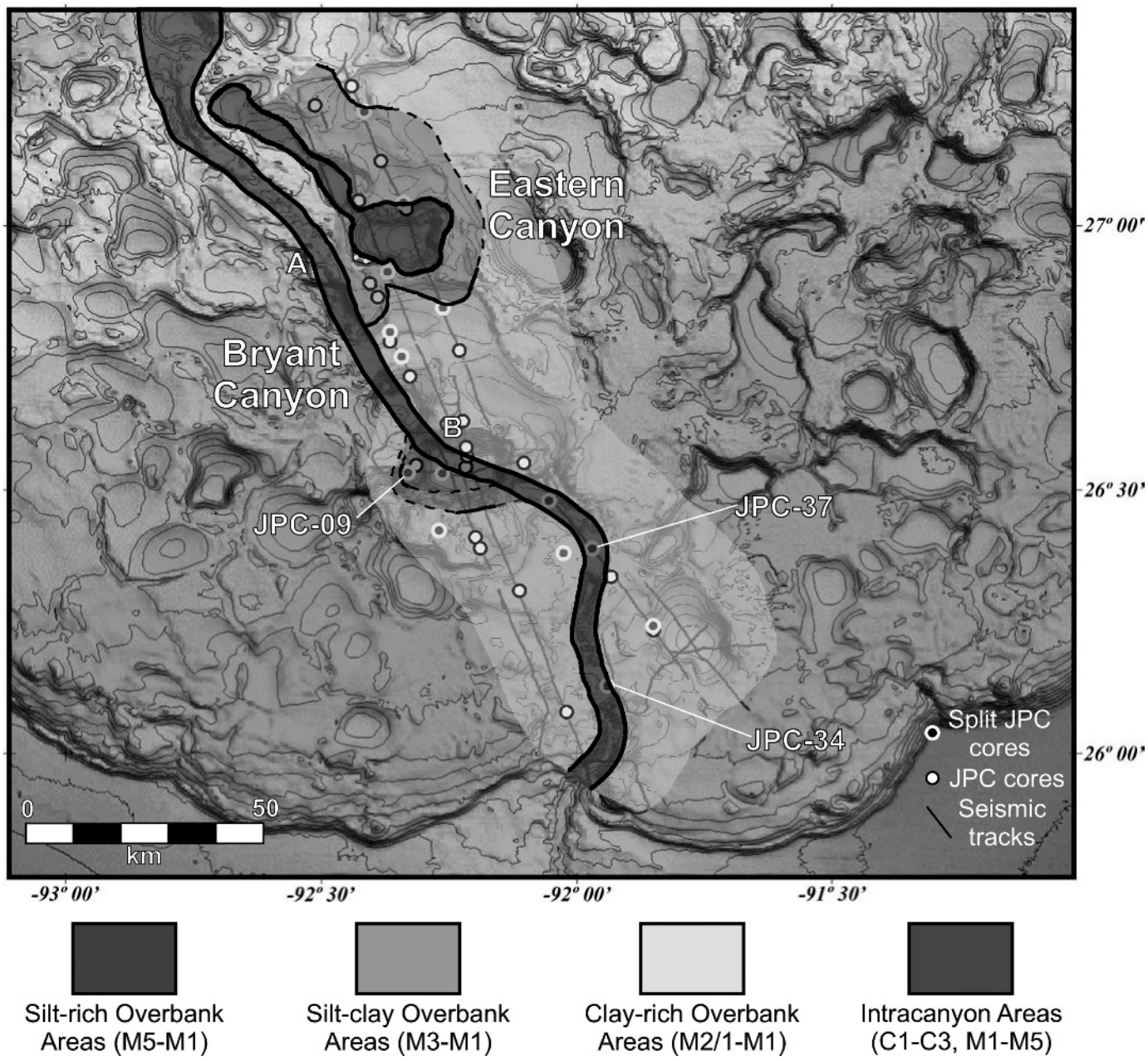

FIG. 11.—Shaded bathymetric map of the Bryant Canyon area displaying the spatial distribution of various turbidite facies deposited during MIS 6. The intracanyon environments (canyon floors) are plotted from the studies of Lee et al. (1996) and Twichell et al. (2000). Discontinuous black lines represent uncertain borders.

interbedded with C1 and C3 facies (Figs. 4, 11), which resemble levee deposits. This indicates that the canyon environment was not exclusively erosional but also had a strong depositional character. Inner levees and terraces, observed in deep-seismic reflection profiles (figs. 5 and 6 in Lee et al. 1996) from Bryant Canyon concur with the erosional–depositional nature of the canyons. This conclusion is consistent with observations from other deltaic prograding slopes (e.g., Ebro Margin; Nelson and Maldonado 1990). There are two possible interpretations, or a combination of them, for the production of inner levees and terraces within a canyon. The first interpretation is through the avulsion of the canyons during periods of low-magnitude turbidity currents (O'Connell et al. 1995; Torres et al. 1997; Wonhamn et al. 2000; Piper et al. 1999b). The second interpretation is through continuous thalweg entrenchment and meander abandonment (Hagen et al. 1994; Von Rad and Tahir 1997; Babonneau et al. 2004).

According to the above discussion, facies C2 and M5 to M1 beds are interpreted to have resulted from small underfit turbidity currents, in which only their upper dilute parts (wash load) were able to overflow the inner levees of the Bryant Canyon. The sand deposits of facies C3 are interpreted to have resulted from the main bodies of large sand-rich turbidity currents, which were able to overflow the canyon inner-levees. Facies C1 can be interpreted as spillover deposits of either the main

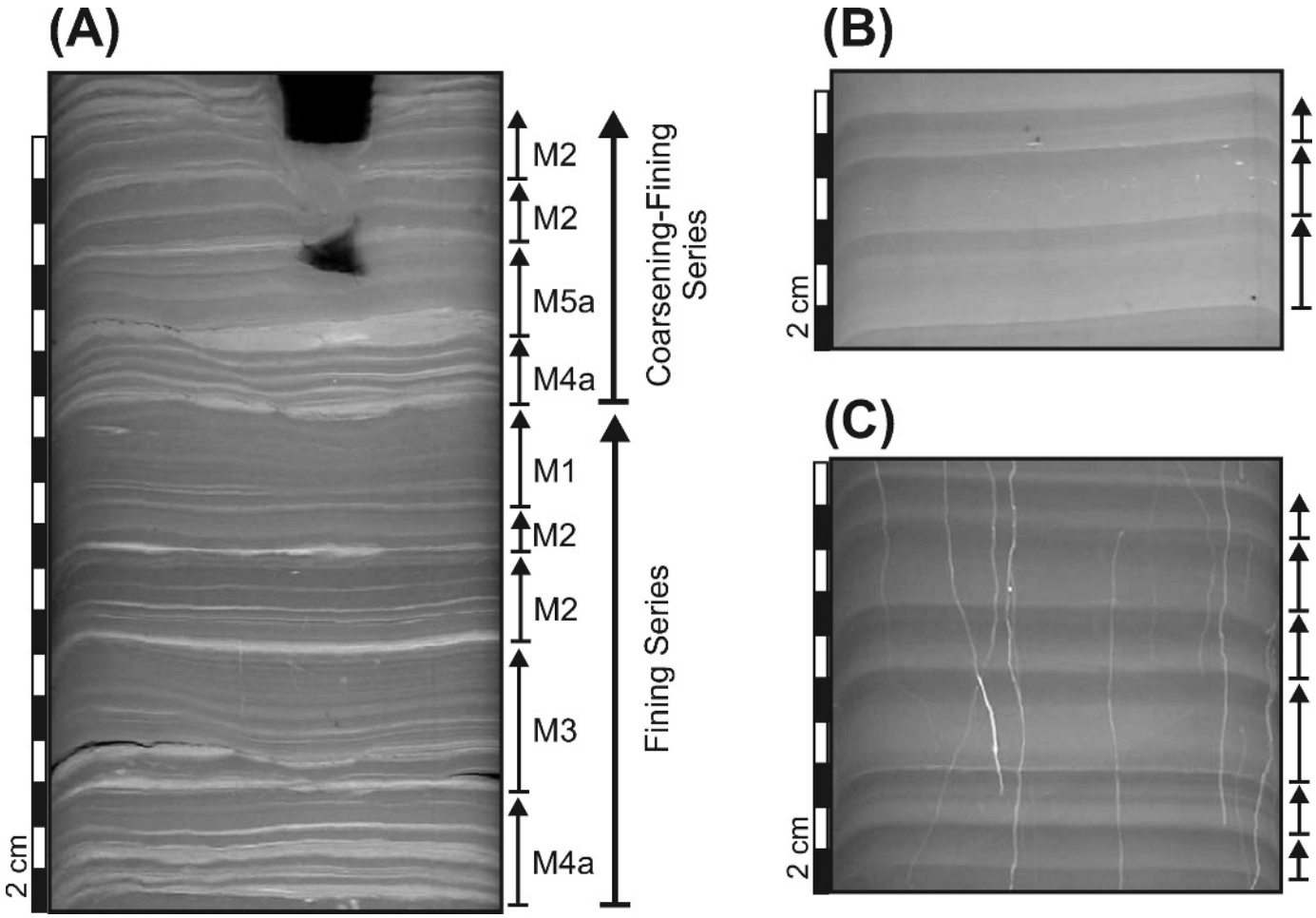

FIG. 12.—X-radiographs (negatives) of: (1) fining and coarsening–fining series of coarse mud turbidite facies (**A**), and (2) fining (**B**) and coarsening-fining (**C**) fine-grained turbidite facies series. The fine-grained facies series consist entirely of M1 facies, where the relative magnitude of their resultant flows is inferred by the thickness and grain size (lighter shades indicate siltier sediments) of the beds.

bodies of silt-rich turbidity currents or the wash load of underfit sand-rich turbidity currents. However, the ungraded nature and almost total absence of sand in facies C1 deposits weakens the second interpretation. The domination of facies C2 and M5 to M1 in the inner levees of the Bryant canyon indicates that underfit turbidity currents were prevalent during the last stage of the canyon.

Areas Subjected to Spillover Processes

It has been shown through this study that, during MIS 6, the overbank areas of Bryant and Eastern canyons have been subjected to intense overflowing and flow-stripping processes, which resulted in the deposition of successive mud turbidite facies (Figs. 4, 5, 6, 11). The large thickness of these deposits ($\geq$ 50 m) in both proximal and distal to the canyons areas, combined with the absence of intercalated hemipelagic sediments, indicates extremely high sedimentation rates. No accurate sedimentation rates can be estimated for MIS 6 overbank deposits, because of the almost complete absence of foraminifera and their age, which is much older than the dating limit of ^{14}C AMS dating (Tripsanas et al. in press). However, a rough sedimentation rate can be implied by the total absence of bioturbation structures at the top of individual mud turbidite beds. The maximum required time for the recolonization of the ocean floor by benthic organisms is five years (Wetzel 1984), inferring that the time interval between two successive turbidity currents was less than 5 years. Based on this assumption, a minimum sedimentation rate of 200–600 cm/ky is estimated for the distal overbank areas of Bryant Canyon.

The mud turbidite facies display a gradual fining away from the canyons (Figs. 6, 11). This information suggests that the spillover flows spread over the low gradients of the overbank areas and acquire a strong depletive character. M1 mud turbidite facies (clay-rich overbank deposits) are the most common deposits around the Bryant Canyon system, indicating that the channelized turbidity currents were sufficiently confined by Bryant Canyon with only their upper most dilute parts (wash load) being capable of overflowing the canyon walls. These very dilute and fine-grained (silty–clay) spillover flows were able to travel for long distances (exceeding 15–20 km), and dictate the sedimentology of the areas surrounding the canyons.

The only exception to the fine-grained nature of the overbank deposits of the Bryant Canyon system occurs along the outer banks of bends A and B of the canyon on the upper and lower continental slope. The sudden intensification of the spillover flows at the bends of the canyon is interpreted by the flow-stripping of the canyon-contained turbidity currents at these locations. The outer banks of bend B consist of facies M5 to M1, which, away from the canyon, grade into M3 to M1 facies and eventually into monotonous M1 facies. The outer banks of bend A consist of M3 to M1 mud turbidite facies that grade into M1 facies away from the canyon. The coarser deposits, occurring at bend B, are attributed to: (1) the intensification of the flow-stripping by the Coriolis

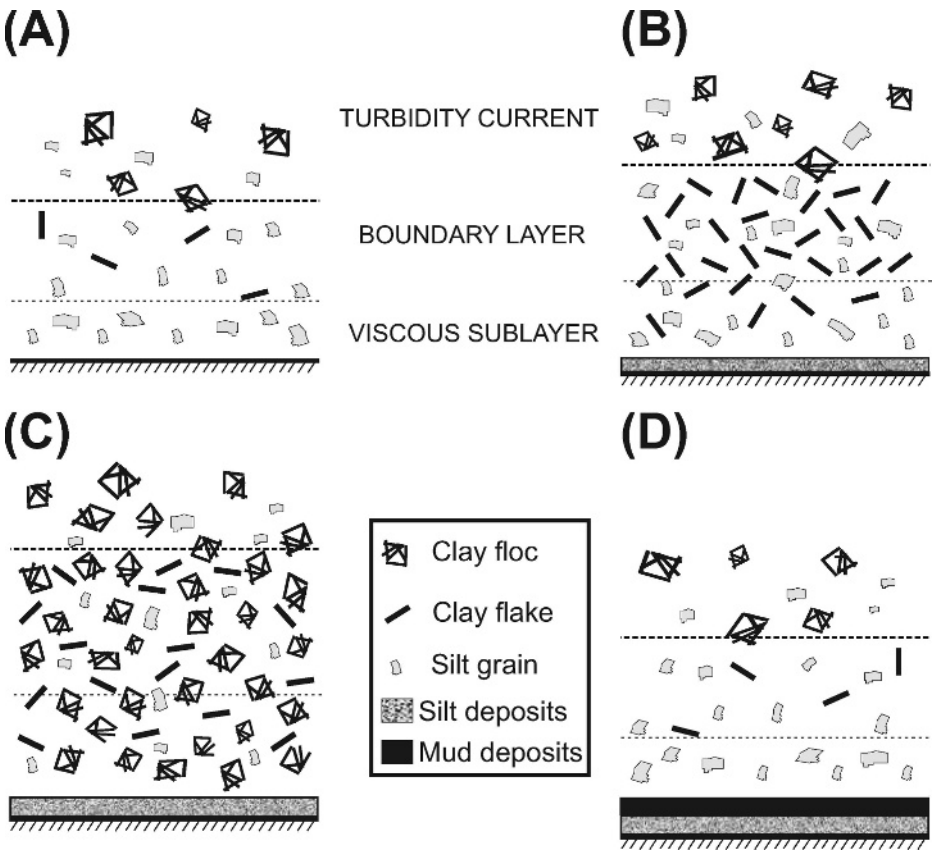

FIG. 13.— Diagram displaying the two-step depositional model that results in the formation of alternating silt and mud laminae (modified from Stow and Bowen 1980): **A)** the shear in the boundary layer leads to the breakage of the settling flocs and allows the deposition of the silt fraction only, **B)** because the amount of clays re-entrained into the overlying flow is less than the settling aggregated clays, their concentration is continuously increased leading to thickening of the boundary layer, reduction of the bursting frequency, and shear reduction within the boundary layer, **C)** the clay (cohesive sediments) concentration in the boundary layer exceeds a critical value, below which the shear in the boundary layer cannot sustain the cohesive sediments disaggregated, leading to their massive deposition (implied by the sharp contacts of the silt and mud laminae), and **D)** the boundary layer is depleted of cohesive sediments (restoration of its initial thickness, bursting frequency, and shear) after their massive deposition and a new depositional cycle is developed.

force (Komar 1969; Bowen et al. 1984; Hay 1987), and (2) a probable lower relief of the canyon at this location. At bend B, the Coriolis force acted in the same direction as the centrifugal force on the turbidity currents, and therefore would have led to the intensification of their flow-stripping. Conversely, the Coriolis force was opposed to the centrifugal force at bend A, and consequently would have suppressed the extension of their flow-stripping.

Eastern Canyon is surrounded by silt–clay overbank areas (M3 to M1 facies) that grade into clay-rich overbank areas (M1 facies) away from the canyon, although it does not display any significant bend. The coarser nature of the Eastern Canyon overbank deposits compared to those of the straight segments of Bryant Canyon indicates that spillover flows in Eastern Canyon were of larger magnitude. Eastern Canyon was confined on the upper continental slope throughout its entire life span, probably due to limited sediment supply. Accordingly, gravity flows were not very abundant in this system, and could not balance the mobilization of the underlying salt masses. Consequently, local highs related to uplifted salt diapirs would have been present along the pathway of the Eastern Canyon system. These morphological irregularities would have forced turbidity currents to undergo successive hydraulic jumps, leading to their thickening and therefore to the intensification of the spillover flows.

The organization of mud turbidite facies into fining and coarsening-fining facies series indicates a cyclicity in the magnitude of the turbidity currents. Given the fluvial source of the turbidites, this cyclicity is attributed to the occurrence of alternating humid and dry periods. In this case, coarsening–fining series represent a gradual transition from dry to humid periods, whereas fining sequences indicate a rather sharp transition. Based on the 5 years maximum recurrence of the mud turbidites, it is concluded that the time scale of these cycles was ranging from annual to a few decades.

Overflowing of turbidity currents occurs when their thickness exceeds the height of the canyon walls. When this condition is met, the sedimentology of the overbank deposits should reveal the nature of their parental channelized turbidity currents. Two types of turbidity currents are distinguished, according to the sedimentological descriptions of the mud turbidite facies. The first and most frequent type is a typical surge-like turbidity current that results in the deposition of normally graded mud turbidite facies. Surge-like flows are most likely generated from the flow transformation of sediment failures (e.g., Hampton 1972; Piper et al. 1999a; Mulder and Alexander 2001). Sediment failures on the front of MIS 6 Mississippi River Delta would be common by analogy to other deep-sea fan systems fed by river deltas (Stow et al. 1996). The second type of channelized turbidity current is characterized by a short waxing initial stage reaching a peak flow velocity (beds with an inversely graded zone at their bases), and then gradually enters into a latter waning stage (normal grading). This type of flow behavior is typical of turbidity currents generated directly from hyperpycnal river plumes (Mulder et al. 2003). Core data reveal that waxing–waning flows occurred only occasionally during MIS 6, and were probably related to periods of exceptionally high river discharges.

Flow Properties

The flow properties of canyon-floor turbidity currents have been estimated according to their structural characteristics and grain-size distribution (Tables 4, 5). Sand-rich turbidity currents, resulting in the deposition of facies C3, were characterized by a velocity of 90–126 cm/s on the inner levees and terraces of the canyon (location of the cores), whereas on the canyon thalweg could be as high as 214 to 267 cm/s. Velocities for silt-rich flows resulting in the deposition of facies C1 are estimated to range between 38 and 86 cm/s (or higher). Sediment

TABLE 4.—*Symbols and equations used in numerical computations.*

B	a coefficient accounting for the mode of sediment transportation (1–1.25: bed load, 1.25–7: suspension, 7–30: wash load)
C	volume concentration of sediment
C_f	drag coefficient at the bed (C_f = 0.0029, Ren et al. 1996)
g	gravitational acceleration
h	thickness of main body of the flow
U	velocity of the main body of the flow
U_*	frictional velocity
$W_{S(d)}$	settling velocity of diameter d sediment particles
α	a factor accounting for the drag at the upper surface of the flow ($\approx$ 0.43)
δ	a factor accounting for the reduction of frictional velocity due to the presence of cohesive sediment in the flows (0.5–0.7 for clay concentrations of 0.1–2 g/l; Best and Leeder 1993; Li and Gust 2000)
ρ	fluid density
ρ_s	sediment density
T	bed shear stress

The following equations of flow are used:

Shields-Bagnold nondimensional boundary shear stress (Allen 1985)

$$\theta = \tau/(\rho_s - \rho)gd \tag{1}$$

(d: modal grain diameter; θ values acquired for the production of each sediment structure are shown in Figure 4.26 in Allen 1985)

The quadratic stress law (Stow and Bowen 1980; Allen 1985)

$$\tau = \rho\delta^2 U_*^2 = \rho\delta^2 C_f U^2 \tag{2}$$

The empirical criteria for sediment transportation (Bowen et al. 1984; Komar 1985)

$$U = BW_{S(d)}/\sqrt{C_f} \tag{3}$$

(d: the 5th and 10th percentile grain-size class)

The modified Chezy type equation (Komar 1969, 1977)

$$U^2 = \frac{(\rho_s - \rho)}{\rho} Cgh \frac{\sin\beta}{(1 + \alpha)C_f} \tag{4}$$

TABLE 5.—*Results of turbidity-current velocities and sediment concentrations based on the sedimentary structure (Equations 1 and 2 in Table 4) and the grain-size distribution (Equation 3 in Table 4) of the turbidites.*

Turbidite facies	Grain-diameter used from the grain population	Grain diameter (μm)	Velocity (cm/s)	Concentration (volume %)
C3	5% (B = 7)	206	267	3–6 × 10^{-4}
C3	10% (B = 7)	184	214	2–4 × 10^{-4}
C3	Mode (B = 7)	149	139	1.6–0.8 × 10^{-4}
C1	5% (B = 30)	38	38	2.8–12 × 10^{-6}
C1	10% (B = 30))	31	26	5.5–1 × 10^{-6}
C1	Mode (B = 30)	20	10	0.8–0.2 × 10^{-6}
Turbidite facies	**Structure**	**Modal diameter (μm)**	**Velocity (cm/s)**	**Concentration (volume %)**
C3	Upper-stage plane formations (θ > 0.5)	149	90–126	3.3–13 × 10^{-5}
C1	Ripple and/or upper-stage plane formations (θ = 0.7–1.7 or higher)	17–20	38–86 (or higher)	0.6–6 × 10^{-5}
C1	Ripple formations (θ = 0.1–0.7)	17–20	14–54	0.1–2.4 × 10^{-5}
M5a	Ripple and/or upper-stage plane formations (θ = 0.7–1.7 or higher)	14–26	33–97	
M4a	Ripple formations (θ = 0.1–0.7)	14–26	12–62	

The sediment concentration of the turbidity currents have been estimated by using Equation 4 in Table 4 and by assuming a flow thickness of 200–400 m based on the remaining morphology of the canyon and other turbidity-current studies involving overflowing and flow-stripping processes (Savoye et al. 1993; Hagen et al. 1994; Klaucke et al. 2000; McHugh and Ryan 2000). The axial gradient of the canyon is ~ 1°. Structural characteristics indicate velocities under which the sedimentary facies were deposited. Velocities based on the grain-size distribution of the turbidites have been formulated to estimate the maximum velocity of the flows (Bowen et al. 1984; Komar 1985). Mud turbidite facies M5a and M4a are placed on the overbank areas of Bryant Canyon (bend B), and no sediment concentration has been estimated for these flows because of their unknown thickness.

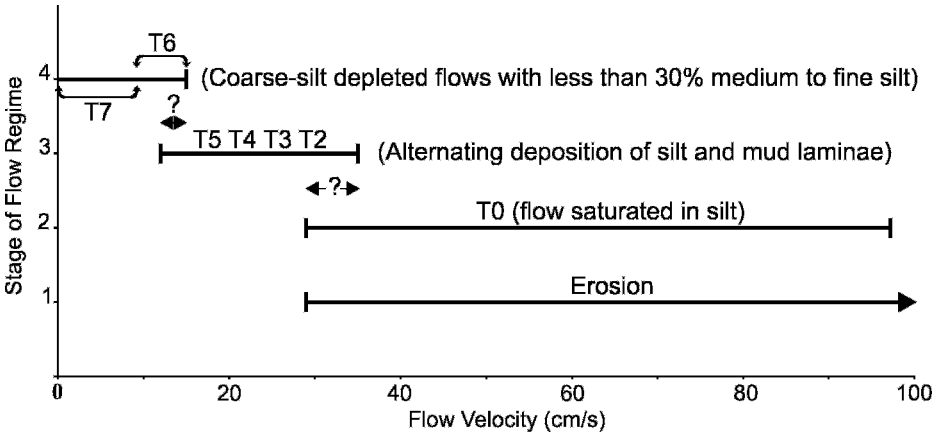

FIG. 14.— Diagram displaying the velocity fields of the four flow-regime stages under which the mud turbidite facies were deposited.

concentrations range from 2×10^{-4} to 6×10^{-4} and 0.1×10^{-5} to 8.9×10^{-5} (volume %) for sand-rich and silt-rich turbidity currents, respectively. In both cases, extremely low concentrations are implicated, resembling those of low-density turbidity currents. This is probably due to: (1) the intense flow stratification of the turbidity currents (Piper and Savoye 1993; Kneller and Buckee 2000), and (2) a significant underestimation of the flow velocities. Deposition of turbidity currents occurs due to loss of capacity and not competence, and consequently, velocities estimated by the grain-size distribution of turbidites may be highly underestimated (Hiscott 1994).

Previous studies of spillover flows, from overbank deposits and mud-wave fields on deep-sea fans, reveal that these flows are characterized by velocities of 10–20 cm/s up to 100 cm/s, thickness of 100–800 m, and low suspended-sediment concentrations of 26 to 2500 mg/l (10^{-5}–10^{-3}) (Normark et al. 1980; Stow and Bowen 1980; McHugh and Ryan 2000; Nakajima and Satoh 2001; Wynn et al. 2000; Gervais et al. 2001). The studies of the above researchers describe the overall properties of a low-density turbidity current. However, each different mud turbidite facies must represent variability in flow conditions. Consequently, the determination of the velocity fields under which each of the flow regimes identified in this study is developed is vital to the better understanding of the temporal and spatial evolution of spillover flows (Fig. 14).

Stage 1 flow regime eroded or sustained all of the sediment in suspension. Because no significant erosion is developed at the bases of the mud turbidite facies M5, we conclude that stage 1 flow regimes were close to an erosional–depositional equilibrium, with velocity higher than 10–25 cm/s. These velocities come from laboratory experiments and represent values above which fine-grained sediments are not deposited (McCave and Swift 1976; Stow and Bowen 1980; Krone 1993).

Stage 2 flow-regime velocities can be estimated from the sedimentary structures (microlaminations and ripples) observed in the basal silt zone of M5a facies, which implies velocity values of 33–97 cm/s (Table 5). The velocity estimates overlap with those of stage 1 flow regime, reflecting the dependence of deposition on the velocity and suspended-sediment-load capacity of the flows.

Stage 3 flow regime is characterized by velocities at which the reentrained cohesive sediments in the main flow are less than those settling in the boundary layer of the flow. Manning and Dyer (1999) and Dyer and Manning (1999) observed in laboratory experiments that there is a critical shear of 0.3 to 0.35 N/m^2 below which the floc size increases with increasing clay concentrations, and vice-versa for higher shear values. Similarly, they observed that the floc settling velocities were highest for the highest clay concentrations at low shear values (< 0.25 N/m^2) and highest for the lowest clay concentrations at high shears (> 0.25 N/m^2). They attributed the decrease of the floc size at high shear and clay concentrations to the higher collision rates of the flocs and their violent interactions that result in floc breakage. Conversely, at low shear values the collisions between the flocs are gentler, leading to their further aggregation and development of higher-order flocs with increasing clay concentrations. Hence, it might be assumed that these critical shear values may also represent a boundary above which the streak-bursting mechanism at the boundary layer overcomes the drag-reduction effects of the cohesive sediments and contributes to their substantial disaggregation and ejection back into the main flow. Consequently, these shear values (0.25–0.35 N/m^2 or 29–35 cm/s) may represent an upper threshold value for the development of stage 3 flow regime. In support of the above velocity values are the silt ripples observed in the silt laminae of facies M4 (T2), which require velocities higher than 12–17 cm/s for their development (Table 5).

The critical grain diameter of 7.8–5.5 μm below which all particles settle as aggregates provides a minimal velocity of 12–13 cm/s (estimated using fig. 1 of McCave and Swift 1976), under which sediment particles of the above critical diameter can be sustained in the flows (Fig. 8). Velocities below these threshold values would cause the deposition of the entire silt population because of the incompetence of the flows. However, spillover flow deposition occurs due to loss of capacity, and consequently velocity values larger than these minimum threshold values are required for the gradational accumulation of silts and clays in the boundary layer, and their cyclic deposition (silt and mud laminae).

Sedimentological descriptions and grain-size analysis of stage 4 flow-regime deposits (M1 facies) reveal that: (1) they are clay-rich ($> 70\%$) and characterized by normal grading, (2) the silt to clayey-silt laminae of the previous stage are replaced by slightly siltier clay to silty–clay laminae, and (3) they are covered by a uniform clay layer. The first two observations indicate that stage 4 flow regimes are: (1) characterized by velocities close to those of the lower limit of stage 3, justifying the presence of silt grains and siltier laminae, (2) highly depleted in the silt fraction, allowing flocculation processes and deposition to dominate in the flows, and (3) gradually decelerating, allowing the development of normal grading. An upper velocity boundary of this flow regime can be estimated from the presence of silt grains up to 31 μm in diameter, which indicate flow velocities up to 15 cm/s (estimated using fig. 1 of McCave and Swift 1976). The third observation implies the existence of a final depositional step, at which the flow becomes incompetent and deposition occurs from an almost stationary sediment cloud.

CONCLUSIONS

Turbidity currents resulted in the deposition of sediments in the Bryant Canyon area during MIS 6. These deposits indicate two sedimentological environments in the area: (1) intracanyon environments, and (2) overbank environments that are widespread along the canyons.

The suspended-sediment load of the channelized turbidity currents consisted of sand and silt or silt with substantial amounts of clay. Turbidity currents during MIS 6 were highly stratified, with the highest concentrations and velocities occurring along the thalwegs of the canyons, developing inner levees and terraces. Typical velocities of the turbidity currents were 38–267 cm/s or higher.

The sedimentology of overbank areas was dominated by low-density spillover flows that resulted in the deposition of thick (> 50 m) successions of mud turbidites. The extension of these deposits is unknown, because MIS 6 mud turbidite successions were present in all core and high-resolution seismic-reflection data. The total absence of bioturbation structures and intercalated hemipelagic sediments indicates that sedimentation rates were extremely high on the overbank areas of Bryant and Eastern canyons during MIS 6, with values succeeding 200–600 cm/ky. Five mud turbidite facies (M1–M5) are recognized from the overbank areas. Most of the mud turbidite facies represent top-cut-out, middle-cut-out (silt-rich facies M5 and M4), and base-cut-out (silt–clay to clay-rich facies M3, M2, and M1) silt–mud turbidite sequences of Stow and Shanmugam (1980).

A complete Stow and Shanmugam (1980) mud turbidite sequence is deposited by the spectrum of four waning-flow regimes. The first two flow regimes are characterized by velocities higher than 29–35 cm/s, whereas in the range of 29–97 cm/s there is an active competition whether erosion or deposition dominates in the flow (Fig. 14). The third flow regime represents a cyclic deposition of silt and mud laminae, due to cyclic fluctuations of the shear in the boundary layer of the flow (12–35 cm/s). The final flow regime is characterized by mud-dominated (flocculation) depositional flow conditions (< 15 cm/s), where graded mud layers are developed. This regime is followed by deposition from a very slowly moving (almost stationary) sediment cloud.

The sedimentary characteristics of the overbank mud turbidite facies provide information not only for the low-density turbidity currents that resulted in their deposition but also for their parental canyon-contained turbidity currents. Surge-like (waning) turbidity currents originating from sediment failures on the front of MIS 6 Mississippi River Delta were the most frequent flows that traversed Bryant and Eastern canyons. However, rare waxing–waning turbidity currents also occurred in these canyons, and were probably related to hyperpycnal river plumes generated during flooding periods of the MIS 6 Mississippi River.

Overbank deposits are organized in fining and coarsening-fining facies series. They are interpreted to represent successive humid to dry climatic cycles. Coarsening-fining series represent a gradual transition between two successive cycles, whereas fining sequences indicate a rather abrupt transition.

ACKNOWLEDGMENTS

This project was sponsored by a National Science Foundation grant to Texas A&M (No. BES-9530370) with supplemental support from Chevron, Mobil, Texaco, Phillips, Marathon, and MARSCO Inc. Part of this work is supported by NRL (contribution no 7430-03-01). We acknowledge the following people for their significant assistance in this project: Armand Silva and Dan Bean for their contribution in collecting the Jumbo piston cores during the Knorr Cruise, 1998; David Prior, Wilford Gardner, and last but definitely not least Arnold Bouma for their help on the development of the above ideas. We would also like to thank David Piper, Bill McCaffrey, Peter Haughton, Hans Nelson, and John Damuth for the thorough review of this paper and constructive comments. Tripsanas acknowledges the S.S.F. Institution of the Greek Republic for funding work on his Ph.D. degree.

REFERENCES

Allen, J.R.L., 1985, Principles of Physical Sedimentology: London, George Allen & Unwin, 774 p.

Allen, J.R.L., 1991, The Bouma division and the possible duration of turbidity currents: Journal of Sedimentary Petrology, v. 61, p. 291–295.

Baas, J.H., Van Dam, R.L., and Storms, J.E.A., 2000, Duration of deposition from decelerating high-density turbidity currents: Sedimentary Geology, v. 136, p. 71–88.

Babonneau, N., Savoye, B., Cremer, M., and Bez, M., 2004, Multiple terraces within deep incised Zaire valley (ZaïAngo Project): are they confined levees?, *in* Lomas, S.A., and Joseph, P., eds., Confined Turbidite Systems: Geological Society of London, Special Publication, v. 222, p. 91–114.

Berryhill, H.L., 1981, Ancient buried submarine trough, northwest Gulf of Mexico: Geo-Marine Letters, v. 1, p. 105–110.

Best, J.L., and Leeder, M.R., 1993, Drag reduction in turbulent muddy seawater flows and some sedimentary consequences: Sedimentology, v. 40, p. 1129–1137.

Bouma, A.H., 2000, Fine-grained, mud-rich turbidite systems: model and comparison with coarse-grained, sand-rich systems, *in* Stone, C.G., and Bouma, A.H., eds., American Association of Petroleum Geologists, Memoir 72, and SEPM, Special Publication 68, p. 9–20.

Bouma, A.H., Coleman, J.M., and Meyer, A.M., eds., 1986, Initial Reports of the Deep Sea Drilling Project Leg 96, Washington, D.C., U.S. Government Printing Office, 824 p.

Bouma, A.H., Roberts, H.H., and Coleman, J.M., 1990, Acoustical and geological characteristics of near-surface sediments, upper continental slope of Northern Gulf of Mexico: Geo-Marine Letters, v. 10, p. 200–208.

Bowen, A.J., Normark, W.R., and Piper, D.J.W., 1984, Modelling of turbidity currents on Navy Submarine Fan, California Continental Borderland: Sedimentology, v. 31, p. 169–185.

Bridge, J.S., 1978, Origin of horizontal lamination under turbulent boundary layers: Sedimentary Geology, v. 20, p. 1–16.

Bryant, W.R., Bryant, J.R., Feeley, M.R., and Simmons, G.R., 1990, Physiographic and bathymetric characteristics of the continental slope, Northwest Gulf of Mexico: Geo-Marine Letters, v. 10, p. 182–199.

Damuth, J.E., 1980, Use of high-frequency (3.5–12 kHz) echograms in the study of near-bottom sedimentation processes in the deep-sea: a review: Marine Geology, v. 38, p. 51–75.

Dyer, K.R., and Manning, A.J., 1999, Observation of the size, settling velocity and effective density of flocs, and their fractal dimensions: Journal of Sea Research, v. 41, p. 87–95.

Fukushima, Y., Parker, G., and Pantin, H.M., 1985, Prediction of ignitive turbidity currents in Scripps Submarine Canyon: Marine Geology, v. 67, p. 55–81.

Gervais, A., Mulder, T., Savoye, B., Migeon, S., and Cremer, M., 2001, Recent processes of levee formation on the Zaire deep-sea fan: Earth and Planetary Sciences, v. 332, p. 371–378.

Hagen, R.A., Bergersen, D.D., Moberly, R., and Coulbourn, W.T., 1994, Morphology of a large meandering submarine canyon system on the Peru–Chile forearc: Marine Geology, v. 119, p. 7–38.

Hampton, M.A., 1972, The role of subaqueous debris flow in generating turbidity currents: Journal of Sedimentary Petrology, v. 42, p. 775–793.

Hay, A.E., 1987, Turbidity currents and submarine channel formation in Rupert Inlet, British Columbia 2. The roles of continuous and surge-type flow: Journal of Geophysical Research, v. 92, p. 2883–2900.

Hesse, R., and Chough, S.K., 1980, The northwest Atlantic Mid-Ocean Channel of the Labrador Sea: II. Deposition of parallel laminated levee-muds from the viscous sublayer of low density turbidity currents: Sedimentology, v. 27, p. 697–711.

Hiscott, R.N., 1994, Loss of capacity, not competence, as the fundamental process governing deposition from turbidity currents: Journal of Sedimentary Research, v. 64, p. 209–219.

Klaucke, I., Savoye, B., and Cochonat, P., 2000, Patterns and processes of sediment on the continental slope off Nice, SE France: Marine Geology, v. 162, p. 405–422.

Kneller, B., 1995, Beyond the turbidite paradigm: physical models for the deposition of turbidites and their implications for reservoir prediction, *in* Hartley, A.J., and Prosser, D.J., eds., Characterization of Deep Marine Clastic Systems: Geological Society of London, Special Publication, v. 94, p. 31–49.

Kneller, B.C., and Branney, M.J., 1995, Sustained high-density turbidity currents and the deposition of thick massive beds: Sedimentology, v. 42, p. 607–616.

Kneller, B.C., and Buckee, C., 2000, The structure and fluid mechanics of turbidity currents: a review of some recent studies and their geological implications: Sedimentology, v. 47(Suppl. 1), p. 62–94.

Komar, P.D., 1969, The channelized flow of turbidity currents with application to Monterey deep-sea fan channel: Journal of Geophysical Research, v. 78, p. 4544–4558.

Komar, P.D., 1977, Computer simulation of turbidity current flow and the study of deep-sea channels and fan sedimentation, *in* Goldberg, E.D., McCave, I.N., O'Brien, J., and Steele, J.H., eds., The Sea, v. 6, p. 603–621.

Komar, P.D., 1985, The hydraulic interpretation of turbidites from their grain size and sedimentary structures: Sedimentology, v. 32, p. 395–407.

Kranck, K., 1975, Sediment deposition from flocculated suspensions: Sedimentology, v. 22, p. 111–123.

Krone, R.B., 1993, Sedimentation Revisited, *in* Mehta, A.J., ed., Nearshore and Estuarine Cohesive Sediment Transport: Washington, D.C., American Geophysical Union, p. 108–125.

Lee, G.H., 1990, Salt tectonics and seismic stratigraphy of the Keathley canyon area and vicinity, Northwestern Gulf of Mexico [Unpublished Ph.D. Dissertation]: Texas A&M University, 182 p.

Lee, G.H., Watkins, J.S., and Bryant, W.R., 1996, Bryant Canyon Fan System: an unconfined, large river-sourced system in the Northwest Gulf of Mexico: American Association of Petroleum Geologists, Bulletin, v. 80, p. 340–358.

Li, M.Z., and Gust, G., 2000, Boundary layer dynamics and drag reduction in flows of high cohesive sediment suspensions: Sedimentology, v. 47, p. 71–86.

Manning, A.J., and Dyer, K.R., 1999, A laboratory examination of floc characteristics with regard to turbulent shearing: Marine Geology, v. 160, p. 147–170.

McCave, I.N., and Swift, S.A., 1976, A physical model for the rate of deposition of fine-grained sediments in the deep sea: Geological Society of America, Bulletin, v. 87, p. 541–546.

McHugh, C.M.G., and Ryan, W.B.F., 2000, Sedimentary features associated with channel overbank flow: examples from the Monterey Fan: Marine Geology, v. 163, p. 199–215.

Mulder, T., and Alexander, J., 2001, The physical character of subaqueous sedimentary density flows and their deposits: Sedimentology, v. 48, p. 269–299.

Mulder, T., Syvitski, J.P.M., Migeon, S., Faugeres, J.C., and Savoye, B., 2003, Marine hyperpycnal flows: initiation, behavior and related deposits. A review: Marine and Petroleum Geology, v. 20, p. 861–882.

Nakajima, T., and Satoh, M., 2001, The formation of large mudwaves by turbidity currents on the levees of the Toyama deep-sea channel, Japan Sea: Sedimentology, v. 48, p. 435–463.

Nelson, C.H., and Maldonado, A., 1990, Factors controlling late Cenozoic continental margin growth from the Ebro Delta to the Western Mediterranean deep sea: Marine Geology, v. 95, p. 419–440.

Normark, W.R., Hess, G.R., Stow, D.A.V., and Bowen, A.J., 1980, Sediment waves on the Monterey fan levee: a preliminary physical interpretation: Marine Geology, v. 37, p. 1–18.

Normark, W.R., Posamentier, H., and Mutti, E., 1993, Turbidite systems: state of the art and future directions: Reviews of Geophysics, v. 31, p. 91–116.

Normark, W.R., Piper, D.J.W., Posamentier, H., Pirmez, C., and Migeon, S., 2002, Variability in form and growth of sediment waves on turbidite channel levees: Marine Geology, v. 192, p. 23–58.

O'Connel, S., McHugh, C., and Ryan, W.B.F., 1995, Unique fan morphology in an entrenched thalweg channel on the Rhone Fan, *in* Pickering, K.T., Hiscott, R.N., Kenyon, N.H., Ricci Lucchi, F., and Smith, R.D.A., eds., Atlas of Deep Water Environments: Architectural Style in Turbidite Systems: London, Chapman & Hall, p. 80–83.

Parker, G., 1982, Conditions for the ignition of catastrophical erosive turbidity currents: Marine Geology, v. 46, p. 307–327.

Peakall, J., McCaffrey, B., and Kneller, B., 2000, A process model for the evolution, morphology, and architecture of sinuous submarine channels: Journal of Sedimentary Research, v. 70, p. 434–448.

Piper, D.J.W., 1978, Turbidite muds and silts on deep-sea fans and abyssal plains, *in* Stanley, D.J., and Kelling, G., eds., Sedimentation in submarine canyons, fans and trenches: Stroudsburg, Pennsylvania, Dowden, Hutchinson & Ross, p. 163–176.

Piper, D.J.W., and Normark, W.R., 1983, Turbidite depositional patterns and flow characteristics, Navy Submarine fan, California Borderland: Sedimentology, v. 30, p. 681–694.

Piper, D.J.W., and Savoye, B., 1993, Processes of late Quaternary turbidity current flow and deposition on the Var deep-sea fan, north-west Mediterranean Sea: Sedimentology, v. 40, p. 557–582.

Piper, D.J.W., Cochonat, P., and Morrison, M.L., 1999a, The sequence of events around the epicenter of the 1929 Grand Banks earthquake: initiation of debris flows and turbidity current inferred from side-scan sonar: Sedimentology, v. 46, p. 79–97.

Piper, D.J.W., Hiscott, R.N., and Normark, W.R., 1999b, Outcrop-scale acoustic facies analysis and latest Quaternary development of Hueneme and Dume submarine fans, offshore California: Sedimentology, v. 46, p. 47–78.

Rabek, K., Ledbetter, M.T., and Williams, D.F., 1985, Tephrochronology of the western Gulf of Mexico for the last 185,000 years: Quaternary Research, v. 23, p. 403–416.

Ren, P., Bornhold, B.D., and Prior, D.B., 1996, Seafloor morphology and sedimentary processes, Knight Inlet, British Columbia: Sedimentary Geology, v. 103, p. 201–228.

Satterfield, W.M., and Behrens, E.W., 1990, A late Quaternary canyon/channel system, Northwest Gulf of Mexico continental slope: Marine Geology, v. 92, p. 51–67.

Savoye, B., Piper, D.J.W., and Droz, L., 1993, Plio-Pleistocene evolution of the Var deep-sea fan off the French Riviera: Marine and Petroleum Geology, v. 10, p. 550–571.

Skene, K.I., Piper, D.J.W., and Hill, P.S., 2002, Quantitative analysis of variations in depositional sequence thickness from submarine levees: Sedimentology, v. 49, p. 1411–1430.

Stanley, D.J., 1983, Parallel laminated deep-sea muds and coupled gravity flow-hemipelagic settling in the Mediterranean: Smithsonian Contributions to the Marine Sciences, v. 19, 19 p.

Stow, D.A.V., and Bowen, A.J., 1980, A physical model for the transport and sorting of fine-grained sediment by turbidity currents: Sedimentology, v. 27, p. 31–46.

Stow, D.A.V., and Shanmugam, G., 1980, Sequence of structures in fine-grained turbidities: comparison of recent deep-sea and ancient flysch sediments: Sedimentary Geology, v. 25, p. 23–42.

Stow, D.A.V., Alam, M., and Piper, D.J.W., 1984, Sedimentology of the Halifax Formation, Nova Scotia: Lower Paleozoic fine-grained turbidites, *in* Stow, D.A.V., and Piper, D.J.W., eds., Fine-Grained Sediments: Deep-Water Processes and Facies: Geological Society of London, Special Publication, v. 15, p. 127–144.

Stow, D.A.V., Reading, H.G., and Collinson, J.D., 1996, Sedimentary environments: processes, facies and stratigraphy, *in* Reading, H.G., ed., Deep Seas, Third Edition: Oxford, Blackwell Science, p. 395–453.

Suter, J.R., and Berryhill, H.L, Jr., 1985, Late Quaternary shelf-Margin deltas, northwest Gulf of Mexico: American Association of Petroleum Geologists, Bulletin, v. 69, p. 77–91.

Suter, J.R., Berryhill, H.L., and Penland, S., 1987, Late Quaternary sea-level fluctuations and depositional sequences, southwest Louisiana continental shelf, *in* Nummedal, D., Pilkey, O.H., and Howard, J.D., eds., Sea-Level Fluctuations and Coastal Evolution: SEPM, Special Publication 41, p. 199–219.

Torres, J., Droz, L., Savoye, B., Terentiev, A., Cochonat, P., Kenyon, M., and Canals, M., 1997, Deep-sea avulsion and morpho-sedimentary evolution of the Rhone Fan Valley and Neofan during the late Quaternary (northwestern Mediterranean Sea): Sedimentology, v. 44, p. 457–477.

Tripsanas, E.K., 2003, Evolution of deposition and slope instability processes on Bryant Canyon area, northwest Gulf of Mexico [Unpublished Ph.D. Dissertation]: Texas A&M University, 154 p.

Tripsanas, E.K., Bryant, W.R., and Phaneuf, B.A., 2004, Slope instability processes caused by salt movements in a complex deepwater environment, Bryant Canyon area, northwest Gulf of Mexico: American Association of Petroleum Geologists, Bulletin, v. 88, p. 801–823.

Tripsanas, E.K., Bryant, W.R., Slowey, N.C., Bouma, A.H., Karageorgis, A.P., and Berti, D., in press, Sedimentological history of Bryant Canyon area, northwest Gulf of Mexico, during the last 135 ky (Marine Isotope Stages 1–6): a proxy record of Mississippi River discharge: Palaeogeography, Palaeoclimatology, Palaeoecology.

Twichell, D.C., Nelson, C.H., and Damuth, J.E., 2000, Late-stage development of a turbidite pathway on the Louisiana continental slope, *in* Weimer, E.D., Slatt, R.M., Coleman, J., Rosen, N.C., Nelson, C.H., and Bouma, A., eds., Deep-Water Reservoirs of the World: SEPM, Gulf Coast Section, 20th Annual Research Conference, CD-ROM, p. 1032–1044.

Von Rad, U., and Tahir, M., 1997, Late Quaternary sedimentation on the outer Indus shelf and slope (Pakistan): evidence from high-resolution seismic data and coring: Marine Geology, v. 138, p. 193–236.

Wetzel, A., 1984, Bioturbation in deep-sea fine-grained sediments: influence of sediment texture, turbidite frequency and rates of environmental change, *in* Stow, D.A.V., and Piper, D.J.W., eds., Fine-Grained Sediments: Deep-Water Processes and Facies: Geological Society of London, Special Publication, v. 15, p. 595–608.

Winterwerp, J.C., 2002, On the flocculation and settling velocity of estuarine mud: Continental Shelf Research, v. 9, p. 1339–1360.

Wonham, J.P., Jayr, S., Mougamba, R., and Chuilon, P., 2000, 3D sedimentary evolution of a canyon fill (lower Miocene-age) from the Mandorove Formation, offshore Gabon: Marine and Petroleum Geology, v. 17, p. 175–197.

Wynn, R.B., Masson, D.G., Stow, D.A.V., and Weaver, P.P.E., 2000, Turbidity current sediment waves on the submarine slopes of the western Canary Islands: Marine Geology, v. 163, p. 185–198.

Received 2 December 2004; accepted 10 December 2005.

APPENDIX A.—*Coordinates, water depth, and core length of the Jumbo Piston Cores (JPC), acquired from the Bryant Canyon area.*

Jumbo Piston Core (JPC)	Latitude	Longitude	Water Depth (m)	Core Length (m)
1	27° 16.79′	−92° 26.402′	1265	13.4
2	27° 3.4′	−92° 20.4′	1450	18.8
3	26° 52.52′	−92° 23.49′	1550	15.6
4	26° 37.89′	−92° 13.494′	1770	15.9
5	26° 35.18′	−92° 12.978′	2220	9.7
6	26° 32.8′	−92° 13.1′	2630	12.5
7	26° 31.78′	−92° 15.96′	2575	4.6
8	26° 31.8′	−92° 19.99′	1685	12.3
9	26° 31.87′	−92° 20.001′	1895	13.1
10	26° 45.52′	−92° 20.65′	1755	15.2
11	26° 32.71′	−92° 18.867′	1740	12.8
12	26° 47.45′	−92° 21.93′	1895	8.9
13	26° 48.24′	−92° 21.94′	2000	16.8
14	27° 3.878′	−92° 25.561′	1400	15.9
15	26° 55.6′	−92° 22.066′	1535	16.4
16	26° 46.29′	−92° 13.82′	1770	17.4
17	26° 32.99′	−92° 6.283′	1945	0
18	27° 8.57′	−92° 22.99′	1355	16.8
19	27° 32.58′	−92° 28.524′	854	16.9
20	27° 32.57′	−92° 28.78′	855	19.2
21	27° 15.59′	−92° 30.6′	1000	17.8
22	26° 54.11′	−92° 24.258′	1475	19
23	26° 45.52′	−92° 20.65′	1760	14.9
24	26° 23.09′	−92° 11.31′	1930	18.9
25	26° 17.89′	−92° 6.921′	1935	14.9
26	26° 22.44′	−92° 1.62′	1995	15.5
27	26° 19.71′	−91° 55.94′	2030	16
28	26° 51.31′	−92° 15.82′	1840	15
29	26° 48.25′	−92° 21.95′	2000	14.3
30	26° 24.24′	−92° 11.84′	1930	15
31	26° 25.13′	−92° 16.162′	1930	15.3
32	26° 43.26′	−92° 19.63′	1915	15.1
33	26° 13.7′	−91° 51.155′	2350	14.6
34	26° 6.599′	−91° 56.4′	2185	14.9
35	26° 3.73′	−92° 1.33′	2230	15
36	26° 13.44′	−91° 50.96′	2355	15.4
37	26° 22.91′	−91° 58.33′	1935	13.5
38	26° 28.73′	−92° 3.25′	2340	0
39	26° 28.73′	−92° 3.25′	2340	10.2
40	26° 34.18′	−92° 12.993′	2525	8.8
41	26° 34.82′	−92° 13.11′	2385	8.4
42	26° 37.65′	−92° 15.181′	1750	9.7
43	26° 46.29′	−92° 13.82′	1770	15.5
44	27° 2.806′	−92° 20.033′	1515	9.91
45	26° 56.31′	−92° 25.46′	1375	16.6
46	27° 3.401′	−92° 20.403′	1450	17.25
47	27° 13.6′	−92° 24.896′	1285	16.6
48	27° 46.04′	−91° 30.78′	545	18.96